2013-04-29

UWB Characteristics of RF Propagation for Body Mounted and Implanted Sensors

Jin Chen
Worcester Polytechnic Institute

UWB Characteristics of RF Propagation for Body Mounted and Implanted Sensors

by

Jin Chen

A Thesis

Submitted to the Faculty

of the

WORCESTER POLYTECHNIC INSTITUTE

in partial fulfillment of the requirements for the

Degree of Master of Science

in

Electrical & Computer Engineering

May 2013

APPROVED:

_____

Professor Kaveh Pahlavan, Major Thesis Advisor

_____

Professor Yehia Massoud, Head of Department

Abstract

Body Area Network (BAN) technology is related to many applications inside, on and around the human body. The basic configuration of a BAN is a set of sensors, which are wearable or are placed inside the human body, transmitting signals to a terminal situated in a doctor's office, in order to assess or monitor some aspect of a patient's physical condition. Additionally, in many BAN applications the information about the sensor location is very important, since without knowing a sensor's location, the transmitted data may be of limited value. As an example, Wireless Video Capsule Endoscopy (VCE) can benefit greatly from the addition of location information. The capsule transmits an RF signal from inside the human body to another sensor on the body surface or external. From the image data provided by the capsule, taken together with the location information, the doctor can locate the infection or lesion and initiate appropriate medical care. In this way, the treatment can be more effective and accurate.

In this thesis we investigate the characteristics of Ultra-Wide Band (UWB) RF propagation for BAN devices placed around and inside the human body. We have made measurements around the human body and around a water-filled phantom using an E8363B Vector Network Analyzer (VNA), specifically measuring the S21 signal, which gives the transfer function. Based on these measurement results, we discuss the channel propagation for cases where the transmitter and the receiver are on the surface of the body and analyze the UWB propagation characteristics for RF localization. Because it is impractical or even impossible to make measurements inside the human body, we chose to apply the measurements using a simulation model of homogenous tissue, which serves as an approximation of the signal propagation environment inside the body. First, by comparing the multipath situation in free space and within a model of homogenous tissue, we are able to analyze the multipath effects inside human body. Then, because of the different characteristics of RF propagation in different bandwidths, we have made measurements at UWB (3GHz to 10GHz), and narrowband (402MHz) frequencies.

Table of Contents

List of Figures

List of Tables

Glossary

AOA	Angle of Arrival
BAN	Body Area Network
CRLB	Cramér–Rao Lower Bound
ECG	Electrocardiogram
FDTD	Finite Difference Time Domain
ISM	Industrial Scientific and Medical
LTI	Linear Time Invariant
MAC	Medium Access Control
MICS	Medical Implant Communication Service
MPC	Multi-Path Components
NIST	National Institute of Science and Technology
POA	Phase of Arrival
RF	Radio Frequency
RMSE	Root Mean Square Error
RSS	Received Signal Strength
RX	Receiver
TOA	Time of Arrival
TX	Transmitter
UWB	Ultra-Wide Band
WBAN	Wireless Body Area Network
WCE	Wireless Capsule Endoscopy
WMTS	Wireless Medical Telemetry
WPAN	Wireless Personal Area Network
WPI	Worcester Polytechnic Institute
WLAN	Wireless Local Area Network
WSN	Wireless Sensor Network

Acknowledgements

In this thesis I describe the research I conducted in pursuit of my Master of Science Degree in Electrical & Computer Engineering at Worcester Polytechnic Institute.

First, I would like to offer my sincerest gratitude to my research advisor, Professor Kaveh Pahlavan, for advising me and supporting me throughout this research. During the one and one half years in the CWINS lab, Prof. Pahlavan offered me many suggestions and valuable advice for my research. Additionally, I have learned a lot from him, not only about how to do research but also about how I can live a happy life. He is a really great man in my mind and I am really lucky to have him as my advisor.

I am really grateful that I can have Professor Allen Levesque and Professor Lifeng Lai as my committee members. Thank you for the valuable comments and reviewing of this thesis. And I also thank Dr. Ning Yang for helping me with the narrowband measurement setup.

I would like to thank Yunxing Ye for his technical help in measurement, understanding of literature and documentation of research. And I also want to thank all my peers in the CWINS lab, Guanqun Bao, Yishuang Geng, Zhuoran (Joanna) Liu, Ruijun Fu, Yadong Wan, Jie He, Pranay Swar, Shen Li and Umair Khan. I thank these people so much for offering me a nice atmosphere in the lab, like a big family.

I would like to delicate my thesis to my beloved parents, who offer me totally understanding, support and infinite love.

Jin Chen

Worcester, Massachusetts

April 2013

Chapter 1

Introduction

Ultra-wide-band (UWB) technology has attracted much attention recently since the announcement of spectrum allocation from 3.1 to 10.6GHz for unlicensed UWB communication applications by the Federal Communication Commission (FCC) [1]. Although product based on UWB Technology have not met the expected results, the UWB channel characteristics have been very helpful for RF localization science and technology [2]. One of the promising applications for UWB technology is Body Area Network (BAN) communications, because UWB is a low-power, high data rate technology. Meanwhile, due to the high center frequency of UWB, the antennas for this band are always small in size, which is a desirable property for body worn devices [3][4].

An important aspect of the development of BAN at UWB is the characterization of the physical layer of the network, including the estimation of the path loss around and through the human body, and delay spread, which are important for communication applications, and time of arrival (TOA) of the first multipath component (MPC) and the received signal strength (RSS) of the first MPC.

There are some BAN applications require the location information of sensors inside or on the surface of human body. A typical one is the wireless video capsule endoscopy (VCE), during the process of examination, the capsules inside human body transmits RF signals to the out surface of human body, and doctors want to know the accurate location of the pill from the information carried by the RF signal. The current technology for locating these sensors is based on received signal strength (RSS) ranging [6], but the accuracy is far from satisfaction. We envision more precise ranging techniques such as TOA ranging will be employed to increase the accuracy of localization results. Unfortunately, there are only a few researchers noticed this

trend and no around or inside human body measurements have been conducted to develop the UWB channel model for localization applications [7-9]. Some other researchers have also done some measurement and analysis around the human body in UWB for the BAN applications [5]. Additionally, a phantom is used in the measurement which mimics the human torso environment is employed to study the effect of human tissue non-homogeneity of localization accuracy [10] [11].

In this thesis, we will focus on developing UWB channel models around human body and inside the homogenous tissue for the body mounted and implanted sensors. The results in this thesis introduce the UWB characteristics of RF propagation for BAN localization around the human body and implanted sensors.

1.1 Motivation

With the development of the health care industry, people pay more and more attention in this area and many applications are created for the BAN. For the BAN, the applications includes the devices on-body, in-body and around human body. These applications can help the doctors to have a better knowledge of the situation inside the patient body and give a quick and accurate treatment. And the wearable sensors connected with wireless network can provide a real time monitor of people's health and in this way the doctors in clinic can find some clues before the patient has emergency lesion. Because of the advantages of UWB technology, there are a lot of UWB applications in BAN area. In order to provide the location information for these applications, people need the channel propagation of the signals in different bandwidth and environment. So we have done the measurement around the human body to figure out the characteristics of the UWB.

1.2 Contribution

During one and half years research at the CWINS Laboratory, I have worked on the measurement for RF localization for BAN applications. I have two major contributions during the research of my thesis. The first one is based on the measurement results around the human body and phantom. Recent research in UWB around human body is focused on the analysis of path-loss model [31], but in my research I have analyzed the UWB characteristics of creeping wave for BAN to provide the location information of body mounted sensors. I published these results in the paper " UWB Characteristics of Creeping Wave for RF Localization around Human Body" in the Personal, Indoor and Mobile Radio Communication (PIMRC), IEEE International Symposium, 2012, which was held in 9-12 September, Sydney, Australia with Yunxing Ye and Professor Pahlavan.

The second major contribution is for the implanted sensors. Obviously, the measurement inside the human body is very difficult to achieve. After analyzing the challenges of measurements using a phantom, we decide to do the measurement inside the homogenous tissue. Different from other researchers who have used to homogenous tissue to do the narrowband measurement and analyze the path-loss model, I am focusing on the TOA and POA technologies which can provide the location information in UWB and narrowband for implanted sensors [40]. Another paper is published in this topic. "Comparison of UWB and narrowband RF Ranging Measurement in Homogenous Tissue for BAN Application" is published in the IEEE wireless Telecommunication Symposium, in April 17-19, Phoenix, Arizona with Yunxing Ye and Professor Pahlavan.

Additionally, there are two more projects I am involved in during the research in the CWINS Laboratory. One is compared the simulation result with the measurement result to find the effect of the bandwidth and distance, which I am cooperated with Joanna Liu. In this project we use the SEMCAD X to simulate the signal transmission inside the homogenous tissue and the human body. The other project is cooperated with UCLA medical school, sponsored by the

Department of Homeland Security. I and Yishuang Geng work together in this project and this project is focused on analyzing the Doppler Spread of the Firefighter's motion in the Bluetooth bandwidth. Based on this Doppler Spread, people can detect the motion of the firefighters to keep them in a safe situation. The information of these two projects will be listed in the Appendix B and C. Additionally, based on the results of these two projects there are two more papers under preparation [60][61].

1.3 Outline of the Thesis

Chapter 1 is an introduction of the basic knowledge of this field. This chapter includes the background of the BAN, the basic location technologies, RF localization, the influence of multipath and different frequency bands for BAN applications (MICS, ISM, WMTS and UWB).

Chapter 2 is a more detailed background of the research I have done.

Chapter 3 describes the measurement scenario around human body, show the measurement result and analyze the measurement result based on the TOA (Time of Arrival of the first peak), RSS (Receive Signal Strength), DME (Distance Measurement Error) and CRLB (Cramer-Rao lower bound).

Chapter 4 describes the measurement scenario inside the homogenous tissue which is a mimic of the environment of human body. The measurements in this scenario are in different frequency band, UWB and narrowband. In this chapter we also analyzed the measurement result in these two bandwidths which can help us to have a better knowledge of the environment inside the human body. And compare the simulation result with the measurement result.

Chapter 5 is the conclusion of the thesis and the future research.

Appendix A includes the all measurement result around the phantom and human body. Appendix B introduces the simulation software, SEMCAD X and compares the measurement result with the simulation result, and the simulation result inside non-homogenous tissue. Appendix C describes the scenario and some measurement results of the project that I and Yishuang Geng cooperate with UCLA.

Chapter 2

Background in Localization for BAN

2.1 Introduction

This chapter describes a general introduction of this research field, including the Body Area Network, channel modeling, RF localization and several frequency bands for BAN. These materials are based on the work of former researchers which inspire me the idea of doing the research in the UWB characteristics.

2.2 802.15.6 Channel Modeling

The development of Wireless Body Area Networking (WBAN) technology started around 1995 with the idea of using Wireless Personal Area Network (WPAN) technologies to implement communications on, near, and around the human body. About six years later, the term "BAN" came to refer to systems where communication is entirely within, on, and in the immediate proximity of a human body. A WBAN system can use WPAN wireless technologies as gateways to extend over longer ranges. Body area network (BAN), also referred to as a wireless BAN (WBAN) or a body sensor network (BSN), is a wireless network of wearable computing devices. The WBAN standard is IEEE 802.15.6, a communication standard optimized for low power devices and operation on, in or around the human body to serve a variety of applications including medical, consumer electronics, personal entertainment and others [12]. In particular, the network consists of several miniaturized body sensor units (BSUs) together with a single body central unit (BCU) [13].

As we mentioned above, The IEEE 802.15.6 TG6 is developing a communication standard optimized for low power devices and operation on, in or around the human body (but not limited to humans) to serve a variety of applications including medical, consumer electronics, personal entertainment and others[12]. Thus in our research, we want to define a channel model that will be helpful in gaining a better understanding of the propagation characteristics of BAN channels. The body area channel is very different from other wireless channels because human body interaction is an integral part of the channel so that the directional channel modeling approaches [26] which are getting more popular in multi-antenna. Recent research in BAN channel modeling has focused on seven scenarios, listed here in Table 1 [27-29].

Table 1: List of Scenarios and Descriptions

Scenario	Description	Channel Model
S1	Implant to Implant	CM1
S2	Implant to Body Surface	CM2
S3	Implant to External	
S4	Body Surface to Body Surface (LOS)	CM3
S5	Body Surface to Body Surface (NLOS)	
S6	Body Surface to External (LOS)	CM4
S7	Body Surface to External (NLOS)	

Based on the scenarios summarized in Table 1, researchers typically build a channel model of RSS, analyze the antenna characteristics, and so on. Because of the differences among the channel configurations in the different scenarios, one may choose different frequency band to do the analysis. Recent researches are always focusing on the scenarios of Channel Model 3 and Channel Model 4, which are Body Surface to Body Surface and Body Surface to External [55]. And this research can be used for the development of the body mounted sensors. In my thesis, I am focusing on the Implant to Implant and Body Surface to Body Surface Scenarios.

As we mentioned earlier, Body Area Network (BAN) describes the application of wearable computing devices, and the frequency bands for BAN include ISM, MICS, UWB and WMTS. Because of the different characteristics of these frequency bands, researchers devise various channel models for the different scenarios. One of the promising applications for UWB technology is BAN communications. In this thesis, we have made measurements around the human body and around a phantom, and in this scenario the character of UWB can be used. An important aspect of the development of BAN at UWB is the characterization of the physical layer of the network, including the estimation of the path loss around and through the human body, and delay spread, which are important for communication applications, and estimation of the time of arrival (TOA) of the first multipath component (MPC) and the received signal strength (RSS) of the first MPC.

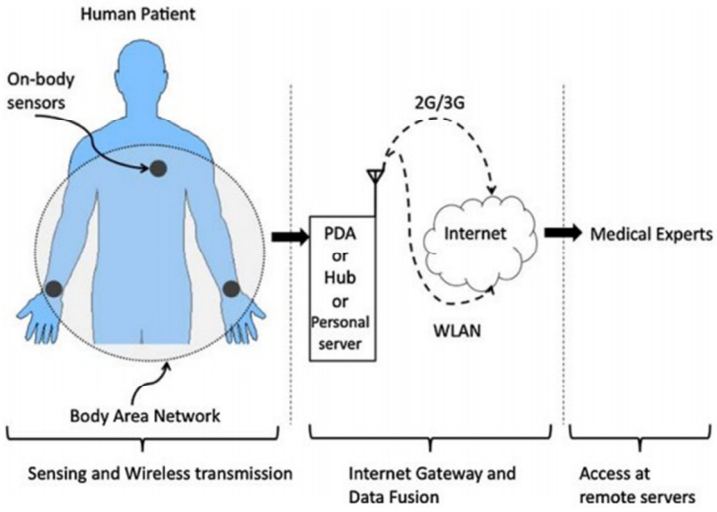

Figure 1: Typical Generic Architecture for Remote Patient Monitoring

Figure 1 shows a typical hierarchical architecture for a patient monitoring system[30]. Generally speaking, the scenario of Figure 1 depicts communication from on- body sensors to external network elements. From Figure 1, the lowest level, the left section of the figure, is a set of wearable or on-body physiological sensors, these sensors forming a BAN. In the middle of the figure is the second level, which is the personal server. The third level is a network of remote health care servers. In this way the experts in clinics can easily access and manage the patient information whether the patient is in the hospital or not.

2.3 RF Localization

As we noted earlier, many BAN applications require location information, and in some cases data sent by the sensors may be useless unless accompanied by accurate location information. This location information can help direct the specialist's attention to the specific site of a tumor, lesion, etc. Wireless Capsule Endoscopy (WCE), for example, needs the location information. The capsule transmits the RF signal from inside human body to the sensor in the surface of the human body or to another sensor inside human body [14].

GPS (Global Position System) is one of the traditional localization technologies. It a space-based satellite navigation system that provides location and time information in all weather conditions, anywhere on or near the Earth where there is an unobstructed line of sight to four or more GPS satellites. GPS has many applications in different areas and it shows a very good performance in outdoor environment. The GPS project was developed in 1973 to overcome the limitations of previous navigation systems, integrating ideas from several predecessors, including a number of classified engineering design studies from the 1960s. GPS was created and realized by the U.S. Department of Defense (DoD) and was originally run with 24 satellites. It became fully operational in 1994. Advances in technology and new demands on the existing system have now led to efforts to modernize the GPS system and implement the next generation of GPS III satellites and Next Generation Operational Control System (OCX). Announcements from the Vice President and the White House in 1998 initiated these changes. In 2000, U.S. Congress authorized the modernization effort, referred to as GPS III [15][16].

But when it comes to the indoor environment, GPS shows its shortcomings. In order to obtain accurate location information, researchers must consider WiFi localization, which is known to provide reliable performance in indoor localization applications.

Figure 2 illustrates the functional block diagram of a wireless geolocation system. The main elements of the system are a number of location-sensing devices that provide metrics related to the relative position of a mobile terminal (MT) with respect to a known reference

point (RP), a positioning algorithm that processes metrics reported by location-sensing elements to estimate the location coordinates of MT, and a display system that depicts the location of the MT to the users. The location metrics may indicate the approximate arrival direction of the signal or the approximate distance between the MT and the RP. There are several metrics we often used in the system, for example, the angle of arrival (AOA) is the metric used for direction, and the time of arrival (TOA), receive signal strength (RSS) and the signal phase of arrival (POA) are used for the distance information [17].

Multipath has a major influence in RF localization. When the signals are transmitted in an urban area, there are many buildings obstructing the path of the transmission, resulting in shadow. This kind of fading, also called slow fading, is well-described by the lognormal distribution, which can be used to calculate the fade margin. Additionally, there is another kind of fading caused by multiple reflection of the transmitted signal. This kind of fading is called multipath fading or fast fading, the latter name used for contrast with shadow fading. Multipath fading is well-described by the Rayleigh distribution [18].

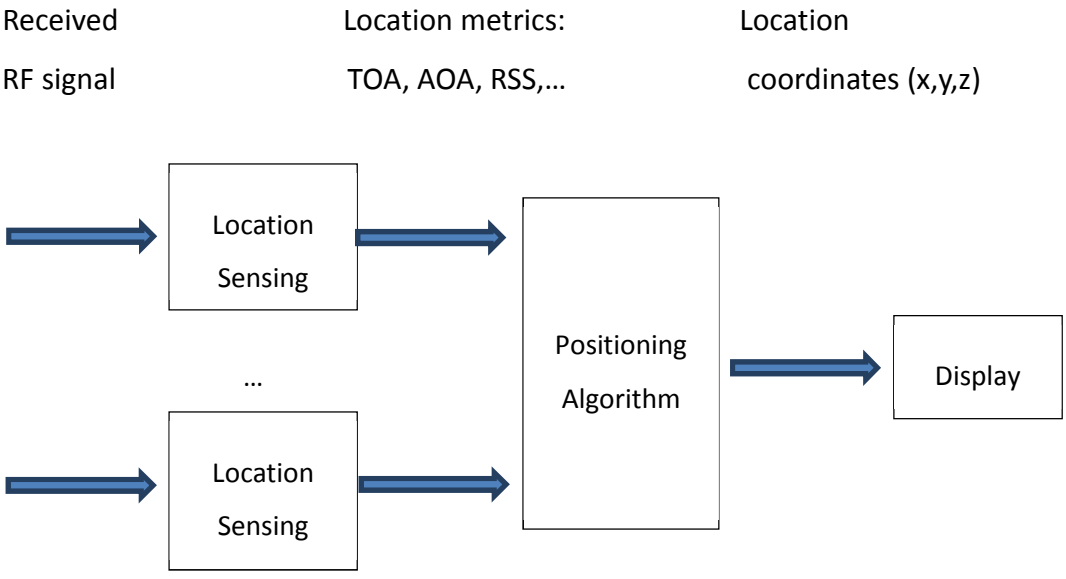

Figure 2: Functional Block Diagram of a Wireless Geolocation System

2.4 Frequency Band for BAN

For Body Area Network (BAN), there are several frequency bands which are always used for the related applications, for example, the MICS band(Medical Implant Communication Service) which is from 402MHz to 405MHz, the ISM band(Industrial, Scientific and Medical) , WMTS band (Wireless Medical Telemetry) and UWB band(Ultra Wide Band). All these bands are defined in the United States by Federal Communications Commission for the transmit data for patient's health. In my thesis, the UWB characteristics are discussed.

Medical Implant Communication Service (MICS) is the frequency band between 402MHz and 405MHz, using for the communication with medical implant. It allows bi-directional radio communication with a pacemaker or other electronic implants. The maximum transmit power is very low, EIRP=25 microwatt, in order to reduce the risk of interfering with other users of the same band. The maximum used bandwidth at any one time is 300 kHz, which makes it a low bit rate system compared with Wi-Fi or Bluetooth. The main advantage is the additional flexibility compared to previously use inductive technologies, which required the external transceiver to touch the skin of the patient. MICS gives a range of a couple of meters [19]. The antenna in the Zarlink development kit is suitable for the MICS band [20]. In the chapter 4 of this thesis, I have done the measurement in narrowband, and the antenna I used in the measurement is also from the Zarlink.

The industrial, scientific and medical (ISM) radio bands are reserved for the use of radio frequency (RF) energy for industrial, scientific and medical purposes other than communications. Examples of applications in these bands include radio-frequency process heating, microwave ovens, and medical diathermy machines. The powerful emissions of these devices can create electromagnetic interference and disrupt radio communication using the same frequency, so these devices were limited to certain bands of frequencies. In general, communications equipment operating in these bands must tolerate any interference generated by ISM equipment, and users have no regulatory protection from ISM device operation. Despite

the intent of the original allocations, and because there are multiple allocations, in recent years the fastest-growing uses of these bands have been for short-range, low power communications systems. Cordless phones, Bluetooth devices, near field communication (NFC) devices, and wireless computer networks all use frequencies allocated to low power communications as well as ISM [21]. There are many different frequency range, bandwidth and central frequency in the ISM band, and recently research for BAN using the ISM band are always in the 2.4MHz to 2.5MHz[22][23].

Wireless Medical Telemetry Service (WMTS) was created in 2000 because of interference issues due to establishment of digital television. The WMTS band has three different frequency bands in US, 608-614 MHz, 1395-1400 MHz and 1427-1432 MHz, but the allocation for it varies from country to country. In Japan, 420–430 MHz and 440–450 MHz are allocated, while 433–435 MHz and 868–670 MHz are used in EU. Because of limitation of the devices, in addition to WMTS, many manufacturers have created devices that transmit data in the ISM bands such as 902-928 MHz, and, more typically, 2.4-2.5 GHz, often using IEEE 802.11 or Bluetooth radios [24].

UWB (ultra-wide band) is a radio technology pioneered by Robert A. Scholtz and others which may be used at a very low energy level for short-range, high-bandwidth communications using a large portion of the radio spectrum. UWB is a technology for transmitting information spread over a large bandwidth, lager than 500MHz. UWB has many applications including non-cooperative radar imaging, sensor data collection, precision locating and tracking applications.

Ultra wideband was formerly known as "pulse radio", but the FCC and the International Telecommunication Union Radio communication Sector (ITU-R) currently define UWB in terms of a transmission from an antenna for which the emitted signal bandwidth exceeds the lesser of 500 MHz or 20% of the center frequency. Thus, pulse-based systems—where each transmitted pulse occupies the UWB bandwidth (or an aggregate of at least 500 MHz of narrow-band carrier; for example, orthogonal frequency-division multiplexing (OFDM)—can gain access to the UWB spectrum under the rules. Pulse repetition rates may be either low or very high. Pulse-based UWB radars and imaging systems tend to use low repetition rates (typically in the range

of 1 to 100 megapulses per second). On the other hand, communications systems favor high repetition rates (typically in the range of one to two gigapulses per second), thus enabling short-range gigabit-per-second communications systems. Each pulse in a pulse-based UWB system occupies the entire UWB bandwidth (thus reaping the benefits of relative immunity to multipath fading, but not intersymbol interference), unlike carrier-based systems which are subject to deep fading and intersymbol interference [25].

Chapter 3

UWB Characteristics of Creeping Wave for RF localization in BAN

3.1 Introduction

In this section, an introduction of some basic technology related to this chapter is given. It includes the UWB technology, the discussion of creeping wave. Some related research is discussed in this section too.

3.1.1UWB

Since the announcement of spectrum allocation from 3.1 to 10.6GHz for unlicensed UWB communication applications by the Federal Communication Commission (FCC), UWB technology has been paid much attention on [1]. Although product based on UWB Technology have not met the expected results, the UWB channel characteristics have been very helpful for RF localization science and technology [2].

As a low-power, high data rate technology, UWB has many applications in lots of areas, such as sensor data collection, precision locating and tracking applications. Based on these characteristics of UWB, one of the applications of it is the BAN. Meanwhile, due to the high center frequency of UWB, the antennas for this band are always small in size, which is a desirable property for body worn devices. Because of all these advantages of the UWB

technology many researchers want to make use of it. Even though some researchers realized that people can use this technology for the BAN, they are not used it for the RF localization [31].

3.1.2 Creeping Wave

The term Creeping wave refers to RF waves diffracted around the shadowed surface of a smooth body such as a sphere. From Figure 3 (this figure from www. intomobile.com), we can clearly get the path which the creeping waves transmitted.

In this chapter, we describe the measurements made in the scenario of body surface to body surface, which can also be described as around human body and phantom. During the measurement we are always facing three kinds of paths when the RF signals transmitting from the transmitter to the receiver. The first kind of path is the direct path (DP). Signal travel through the water in the phantom or human tissue in real body to reach the receiver .These paths are not the dominant path in BAN scenario because of the sever gain reduction from water or body tissue, we tend to neglect these paths in practice because they are too weak to be differentiated from background noise by the receiver [31]. The frequency band in the measurement is UWB, which is between 3 GHz and 10GHz in which the diffraction is much stronger. The second kind of path is diffraction around the human body or phantom which is also called 'creeping wave'. We will focus our discussion on these paths due to most availability of them in the body surface to body surface scenario. The third kind of paths is the reflections from the environment which can also be neglected because we did all the measurements in the chamber in order to kill the other interfering MPCs [22].

Based on the all the analysis above, in this chapter we will only focus on the second path, the creeping wave, which are the main path in our measurement to develop the channel model for RF localization for BAN applications. For the creeping wave, we may also have multipath, but the path around the human body is the shortest and the one provided the first peak which can be used to calculate the time of arrival.

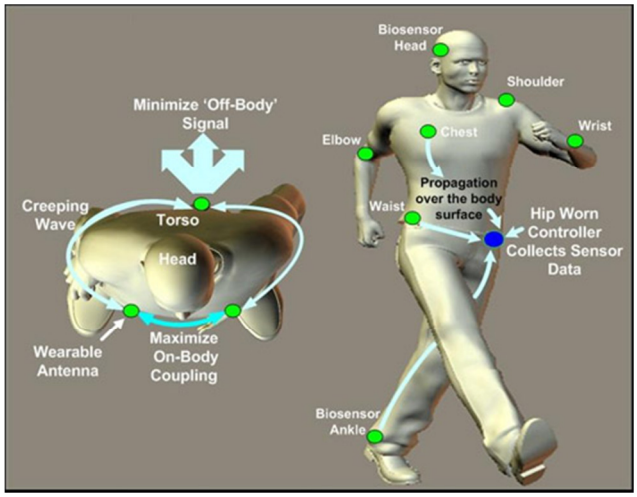

Figure 3: Creeping Wave Model

3.2 Measurement Setup and Scenario

The measurement setup is configured for conducting the measurements around the human body and a phantom to develop UWB channel model for various MPC parameters such as TOA, RSS and total path-loss [32] for RF localization.

All the measurements presented in this chapter were conducted in an RF anechoic chamber, a shielded room, having dimensions 2.32m × 2.41m × 2.29m. The interior structure of the chamber greatly attenuated any MPCs reflected from walls, and also isolates the experimental setup from RF signals existing outside the chamber. An E8363B Vector Network Analyzer (VNA) is employed to sweep the frequency from 3-10GHz. The measurement parameters are listed in Table 2.

We measured the transfer function (S21) and the measurement results are stored in a PC which is wirelessly communicated with the VNA. After obtaining the frequency data, we first apply a Hamming window to the data to reduce the effect of side lobes and then use the Inverse-Chirp Z transform to convert the frequency data to a time domain impulse response.

After that, we apply a peak detection algorithm to extract the MPC from the time domain impulse response and analyze the parameters in time domain. The measurement scenario using VNA and UWB antenna are shown in Figure 4.

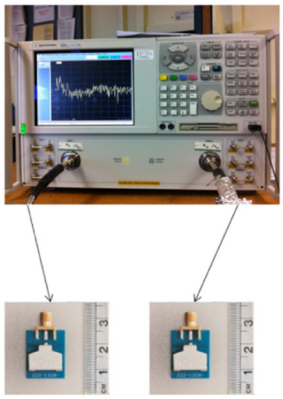

Figure 4: Measurement using VNA and UWB Antenna

Two antennas are used during the measurement campaign. The antennas used in this measurement are model SMT-3TO10M-A UWB patch antennas from SkyCross corporation [33], shown in Figure 5. The operating frequency range of this antenna is between 3.1 and 10.0 GHz. The antennas and the VNA are connected by shielded coaxial cables. There may be some power loss in the connection part. And to eliminate the loss from the coaxial cables we use Tin Foil as better shielding to cover the cables and the connection part between the antenna and the VNA.

Table 2: Measurement Parameters

VNA setup parameters	value
Frequency band	3-10GHz
Number of points	1601
Transmission power	0dBm

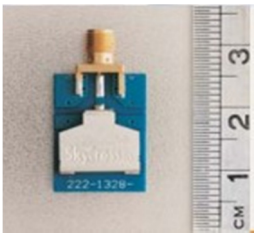

Figure 5: UWB Antenna from SkyCross

Figure 6(a) shows the measurement setup around a phantom filled with water. The phantom we used in the measurement is from the Phantom Laboratories [34]. The surface of the phantom is made by cellulose acetate butyrate. During the measurement, the phantom is filled with water in order to simulate the simplified environment of human body because the electrical characteristics of human tissue are close to water. We did the same amount of measurements at three different height and seven receiver location points in each height as show in Figure 7. We conducted 20 measurements at each receiver location to study the statistics of MPC parameters. The total length from the shoulder to the waist is 45cm, hence we did the measurements every 15cm which are shown in the Figure 6(a) as Height A, Height B and Height C.

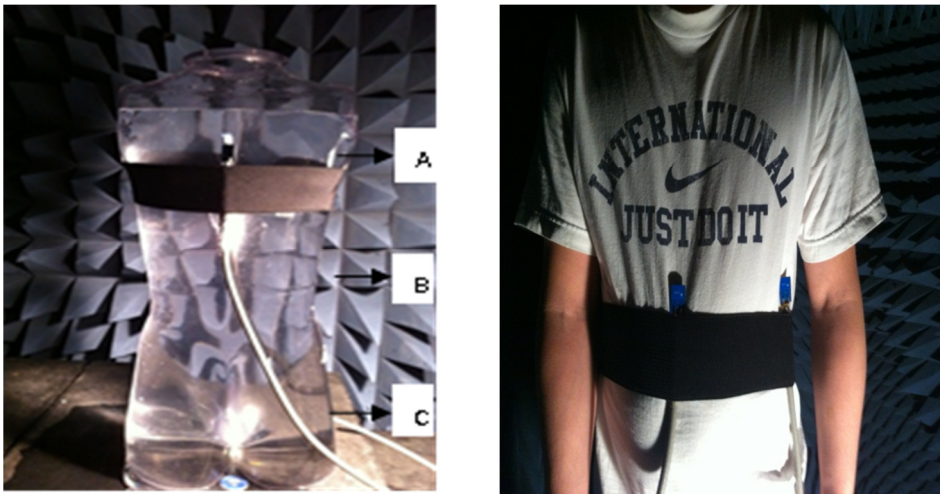

Figure 6: (a) Measurement Setup around Phantom (b) Measurement Setup around Body

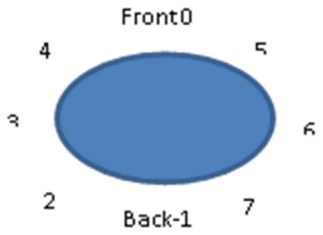

Figure 7: Locations of the Measurement Points Every Height

The transmitter antenna is fixed on the front surface of the human body or a phantom, as point 0 shown in Figure 7. The distance between the human body and the antenna is around 10mm, which is caused by the clothes of the subject. The distance between the phantom and the antenna is also 10mm, because the cable is fixed next to the phantom, and in this way there is a room between the antenna and the phantom. The distance between every two adjacent points is equal. We also did the similar measurements around the human body, shown in Figure 6(b). During the real human body measurements the person is in a standing position and tries to keep static during the process of data collection.

3.3 Measurement Results

In this section, we will show the measurement results, which include four parts: calibration of measurement, measurement with empty phantom, measurement with phantom filled with water and measurement around human body. The calibration of measurement is needed because there is a system bias which may be caused by the cable connected with the Vector Network Analyzer. The measurement in the empty phantom can help us to analyze the first peak which is proved from the creeping wave. All these measurements were made in the shielded chamber described above in order to kill the influence of the reflection of the walls and ground.

3.3.1Calibration of Measurement

Because the system bias exists, it is necessary to measure the TOA in free space as a reference distance between the two antennas in order to determine the system bias. The measurement result in the free space is shown in Figure 8(a) and (b), and part (b) zooms in on the result so that we can read it more clearly. From the measurement result there is only one path, because it is measured in the chamber and the only path is the direct path (DP). In this calibration measurement, the expected distance between the transmitter and the receiver is 23.5cm, and the distance actually measured between transmitter and the receiver is 30cm. In this way we can calculate the system bias as follows:

$$\Delta t = \frac{D_E}{c} - \frac{D_M}{c} \tag{1}$$

In equation (1), c is the speed of light, D_E is the expected distance between the two antennas, D_M is the measured distance by the VNA. From (1), we can have that the system bias is 0.25ns.

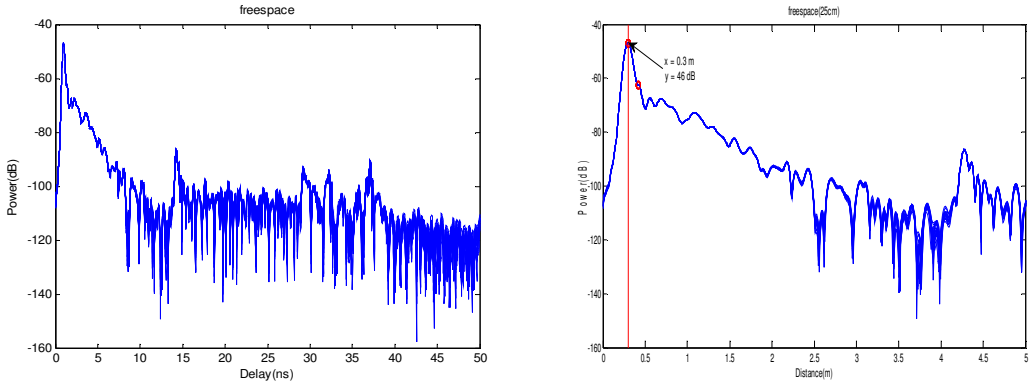

Figure 8: (a) RSS in Free Space from 0 to 50 ns; (b) RSS in Free Space from 0 to 5ns

3.3.2Measurement Results

After finding the system bias of the VNA, we can acquire more accurate results in our measurements. In this section, three measurements have been done. Firstly, we need to prove

that the first peak is from the creeping wave instead of the direct path. In order to make this assumption solid, we compared the measurement result of phantom filled with water with the measurement of the empty phantom. From Figure 9 (a) we can find that the first peak, at the same time the strongest peak, is really close to the expected time of Line of sight (LOS). In this way we can tell that the first peak is from the direct path (DP) when the antenna is attached around the empty phantom.

In the Figure 9 (b), the red line is the expected time of the creeping wave, and the blue line is the expected time of direct path. Direct path needs more time to reach the receiver because the signal needs to transmit through the water, and inside the water the transmit velocity is much smaller than that in the free space, formula (2). And in the formula (2), c is the velocity of light and $\varepsilon_{r(\omega)}$ is the permittivity of water.

$$\mathrm{v}(\omega) = \frac{c}{\sqrt{\varepsilon_{r(\omega)}}} \tag{2}$$

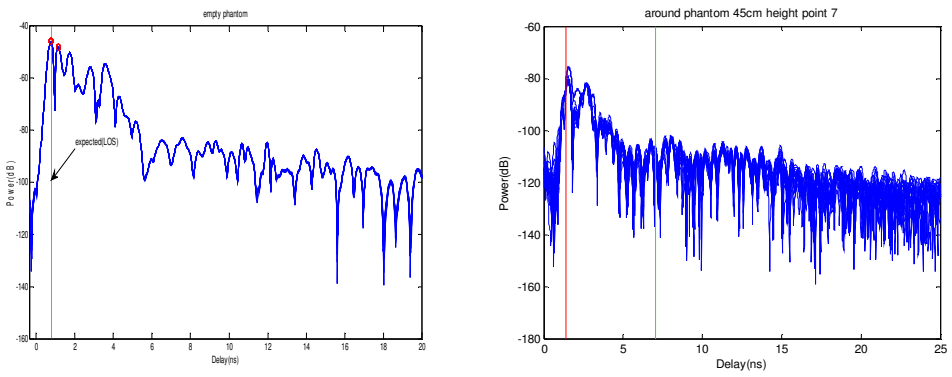

Figure 9 (a): Measurement Result with Empty Phantom; (b): Measurement Result with Phantom Filled with Water

In Figure 9(b), we can find that creeping wave has multipath. The several peaks following the first one are all from the creeping waves, because we do this measurement in a shielded chamber, there is no refection from the walls or the ground. The longest way from the transmitter antenna to the receiver antenna should be the path past the shoulder. This distance is nearly 95cm, and in this way the transition time is around 3.12 ns.

The measurement with phantom filled with water is done in three heights and seven points each height. In this way, we can analyze the multipath situation of the phantom filled with water. The horizontal ordinate in these figures is the transition time, and vertical coordinates in these figures is the receive signal strength. The measurement results around phantom are shown in Figure 910(a). The measurement result in Figure 10 (a) is the one when the receiver in point 7 and at the height of 45cm around the phantom. From Figure 10 (a) we can tell that the peaks in it, the first one is from the shorter creeping wave, and the other is from the longer one. The power of peak from the shorter creeping wave is much larger than that from the longer one. Additionally, we also calculate path from the DP, and the expected arrival time is around 7ns, and from the Figure 10 (a) we can conclude that the direct path cannot be found from the noise.

The measurement around human body is also done in three heights and seven points each height. We choose the measurement result when the receiver in point 3 at the height of 45cm around the human body. The example of the measurement results around human body is shown as follows in Figure 10 (b). And from Figure 10 (b), we can tell that there is no other path except the multipath from creeping wave, because there is no reflection in the chamber.

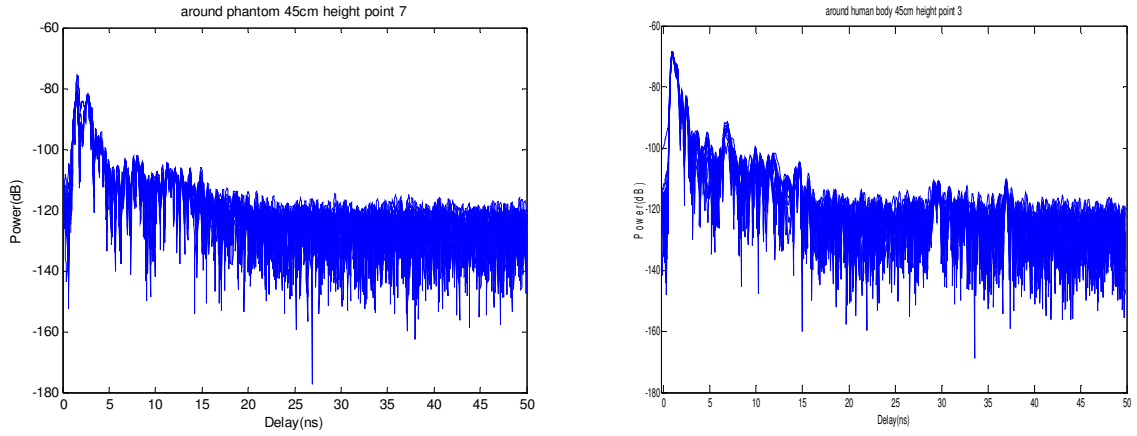

Figure 10: (a) Measurement Result around Phantom (b) Measurement Result around Human Body

3.4 Analysis of the UWB Characteristic of Creeping Wave

By obtaining the measurement result above, in the following part UWB characteristics of creeping wave will be analyzed. For the RF localization applications around the human body, we develop UWB channel models based on several important metrics, such as the total path-loss which is for RSS based localization, TOA and gain of the first arrived MPC in order to obtain the location information.

- Time of Arrival: τ_i (3)
- Power of the First Peak: $P_{FP} = \alpha_i$ (4)
- Total RSS: $P_t = \sum|\alpha_i|^2$ (5)
- Impulse Response: $h(t) = \sum \alpha_i \, \delta(t - \tau_i)$ (6)

From the formula above (3-6), the time of arrival means the arrival time of the first path. And the total receive signal strength adds all the power of the peaks above the noise, which we assume it as -110dB. And in this section, we will be built the angle based model. The angle in the models means the angle between the transmitter and receiver, shown in Figure 11.

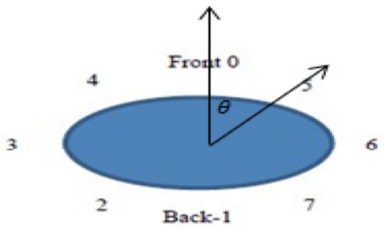

Figure 11: Angle between Transmitter and Receiver

3.4.1Modeling the Time of Arrival

Time of arrival(TOA) is an important ranging metric for localization in Body Area Network(BAN), and the TOA of the first peak in the channel profile can be directly convert to distance information as the input to localization estimation algorithms.

During this part of the measurements, the phantom is filled with water, and the first path is the path diffracted around the phantom as we approved before. Table 3 shows the circumference in different height of both human body and phantom, from which we can find that these two only have slightly different with each other. Because of the differences in the distance from point 0 to the same point in different height, we decide to use angle instead of distance as the reference. Table 4 shows the degree of the angle from the transmitter antenna to receiver antenna.

Table 3: Different Circumference in Different Situations

Circumference(cm)	Human body	Phantom
Height A	96	96
Height B	90	84
Height C	88	88

Table 4: Degree of the Angle from P0 to Pn

P 0 to	P 1	P 2	P 3	P 4	P 5	P 6	P 7
Angel (degree)	180	132	90	48	312	270	228

We have three groups of data obtained in different heights, and for the same angle the expected TOA are different because of the difference in circumference in different height. So we calculate the arithmetic square root of the TOA of every three points in same angle but in different height. In this way, we can use to compare the measured TOA and the expected TOA using angle based model.

$$TOA_{Ex} = \frac{D_{0n}}{C} + \Delta t \tag{7}$$

$$\tau(\theta) = \begin{cases} \alpha \times \frac{\theta \times \pi}{180} + \Delta t; & 0 < \theta < 180 \\ -\alpha \times \frac{(\theta - 360) \times \pi}{180} + \Delta t; & 180 < \theta < 360 \end{cases} \tag{8}$$

Because the expected TOA of the first peak can be treated as transmissions time of signal though the path around the surface of human body or of the phantom. And generally, the expected TOA are calculated using the distanced based model, (7). In this formula D_{on} means the distance from transmitter point 0 to the receiver antenna point n, c is the speed of signals via air and Δt means the system bias which equals to 0.25ns. Based on our measurement result, we calculate the expected TOA of the first peak using the angle based model, as shown in (8). In (8), $\propto$ equals to 1/2, and Δt equals to 0.25ns.

In Figure 12 (a), the circle points are the measured TOA and the starlike points are the TOA calculated using the angle based channel model. The vertical axis in Figure 12 (a) is the angle between the transmitter and the receiver, and the horizontal axis is the TOA of the first peak. From the Figure 12 (a) we notice that the measured TOA and the expected TOA are very close. The first peaks in different points in different height are always the strongest peak in our cases.

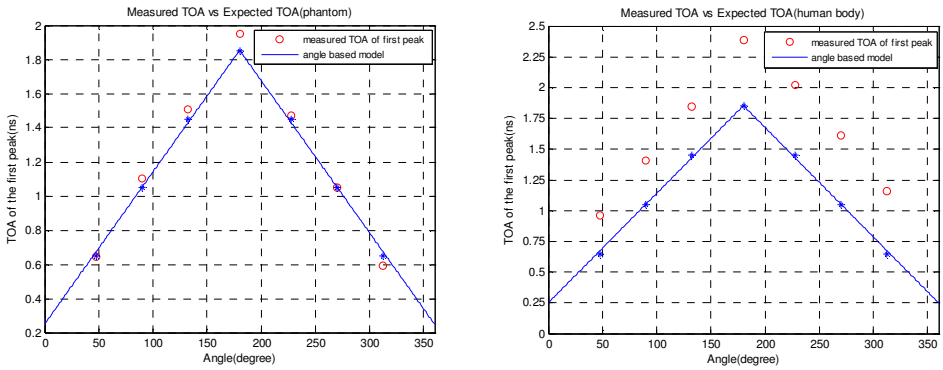

Figure 12: (a) Comparison of Measurement TOA and Expected TOA around Phantom. (b) Comparison of Measurement TOA and Expected TOA around Body

Figure 12 (b) shows the TOA of the first peak around the human body. The main path we interested in is the creeping wave, which may be influenced by the environment of the surface. The expected TOA of each angle is also used the same angle based model (8). From the measurement results we can find the TOA error of the human body is larger than it of the phantom. But the different between the angle based model and the measurement result around the human body has almost the same in each point. This result is reasonable because the measurement circumstance of human body is more complex than it of phantom.

3.4.2Distance Measurement Error

The accuracy of localization based on TOA is highly related with DME. We calculate and plot the DME to figure out its distribution around the human body and around the phantom. The definition of DME is as follows [35]:

$$\varepsilon = \hat{d} - d \tag{9}$$

In (9), $\hat{d}$ means the measured distance between the transmitter and the receiver, and d means the expected distance between the transmitter and the receiver. The circles in Figure 13(a) show the DME of each point around the human body, and the starlike points show the DME of each point around a phantom. In Figure 13 (b), it plots the DME of creeping wave in a linear scale versus distance. From Figure 13 (b), we found that the trend and gradient of the

DME around human body and around the phantom are very close. So the big DME of the measurement around human body is caused by the influence of the surface, which we can treat it as a bias.

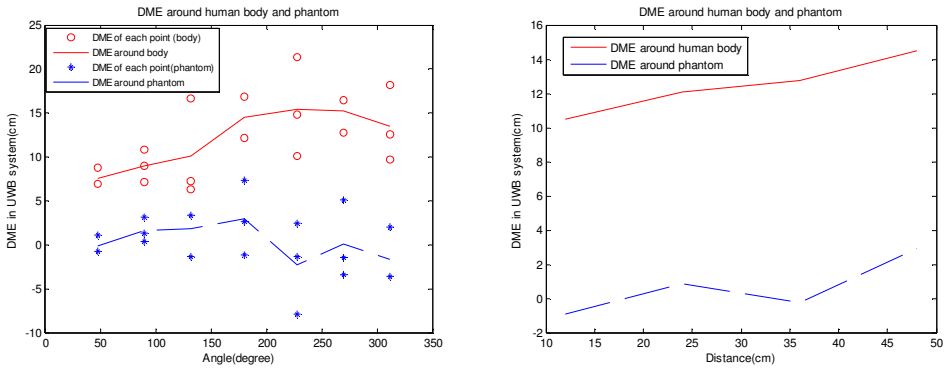

Figure 13: (a) DME of Creeping Wave versus Angle around Body and Phantom (left) (b) DME of Creeping Wave versus Distance around Body and Phantom

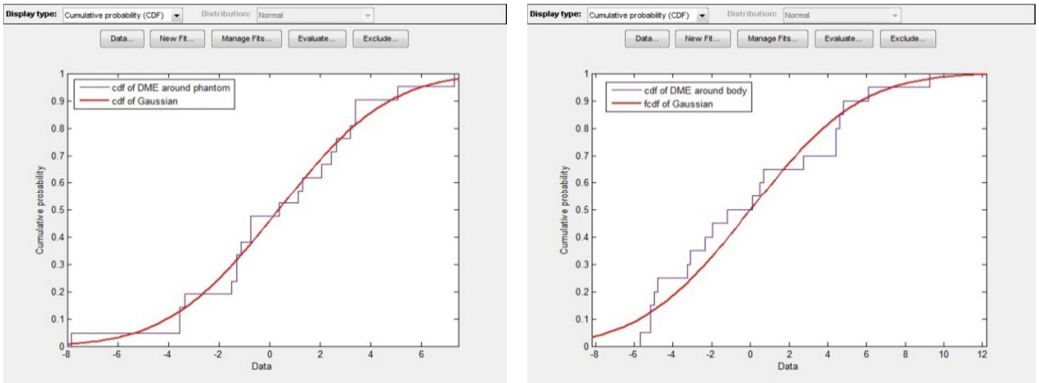

Figure 14: (a) Comparison the CDF of Gaussian and CDF of DME around Phantom (left) (b) Comparison the CDF of Gaussian and CDF of DME around Body

From Table 5, we can find that mean of DME around a phantom is close to 0. And using the distribution-fitting tool of MATLAB we can find that the DME around a phantom is according with Gaussian distribution which is shown in Figure 14(a). The mean of DME around human body is 12.06 and from Table 5 we can find that there exists a bias which can be treated as 12.06cm. After eliminate the bias, we compare the CDF (Cumulative Distribution Function) of DME around human body and Gaussian distribution as shown in Figure 14(b), and these two lines fit well.

Table 5: Mean and Standard Deviation of DME around Human body and Phantom

	DME	
	Mean	Std.
Human body	12.06	4.46
Phantom	0.34	3.44

3.4.3Bounds on Ranging Error

The Cramer-Rao lower bound (CRLB) is helpful to investigate the achievable accuracy limits for TOA based localization, so it is needed to determine the relationship between the DME in TOA and the error in TOA localization.

From [36], we can have two inequalities, (10) and (11). (10) is the Cramer-Rao lower bound (CRLB) for a distance estimate $\hat{d}$ from RSS measurements. And (11) is the best achievable accuracy of a distance estimate $\hat{d}$ from TOA. In these formulas, d is the distance between the two antennas, n_p is the path loss factor, and σ_{sh} is the standard deviation of the zero mean Gaussian random variable representing the log-normal channel effect. But in our measurements, the DME is calculated based on the TOA, in this way we use (11) instead of (10) to calculate the CRLB, which estimate the distance from TOA.

$$\sqrt{Var(\hat{d})} \geq \frac{ln10}{10}\frac{\sigma_{sh}}{n_p}d \tag{10}$$

$$\sqrt{Var(\hat{d})} \geq \frac{c}{2\sqrt{2}\pi\sqrt{SNR}\beta} \tag{11}$$

$$\beta \triangleq \left[\int_{-\infty}^{\infty} f^2|S(f)|^2 df \Big/ \int_{-\infty}^{\infty}|S(f)|^2 df\right]^{1/2} \tag{12}$$

In (11), c is the speed of light, SNR is the signal-to-noise ratio, and β is the effective signal bandwidth which is defined in (12). Because the receive power of the first peak of the creeping waves is from -45dBm to -90 dBm, and the power of noise is close to -120dBm. In this way, SNR is to from 75dB to 30dB. β equals to 7 GHz. Based on (11), the standard deviation is less than 0.11cm which is much smaller than the minimum measured standard deviation, 2.32cm. So the inequality (11) established. In Figure 15 (a) and (b), the comparisons of the DME and CRLB around phantom and around human body are shown. We can find from the Figure 15 that there is a difference between the DME and CRLB, which may be caused by the noise of signal and grid of VNA.

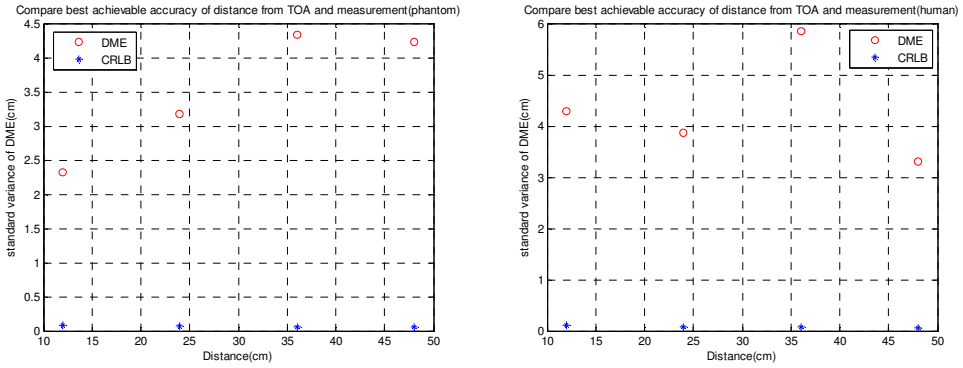

Figure 15: (a) Comparison of Best Achievable Accuracy of Distance from TOA and Measurement around Phantom (b) Comparison of Best Achievable Accuracy of Distance from TOA and Measurement around Body

3.4.4Modeling the Path-loss for the First Path

RSS of the first peak is an important factor in RF localization. Only using RSS of the first peak to estimate the location, the result may have a big error with the actual location. But if the first peak can be captured accurately, we can estimate the location of the transmitter antenna with the help of the TOA.

In our measurement, the selected points around human body and phantom are symmetrical, and in this way we can combine the data from two sides. Based on the measurement results, we can build an angle based channel model for the path-loss of the first peak as follows (13):

$$P_{f-dB}(\theta) = P_{dB}(\theta_0) - \gamma_1(\theta - \theta_0) \quad (13)$$

Figure 16(a) shows the path-loss of the measurement points and angle based channel model we built of the first peak around a phantom, and the circles are the path-loss in different angle. Figure 16(b) shows the path-loss of the measurement points and the angle based channel model we built of the first peak around the human body. Figure 17 plots these two path-loss model in one figure in order to do the compare.

Table 6: Parameter of Angle based Channel Model of the First Peak Path-loss

	Phantom	Human
$P_{dB}(\theta_0)$	41.25 dB	48 dB
γ_1	16dB/rad	18dB/rad
θ_0	0.2415 rad	0.2415 rad

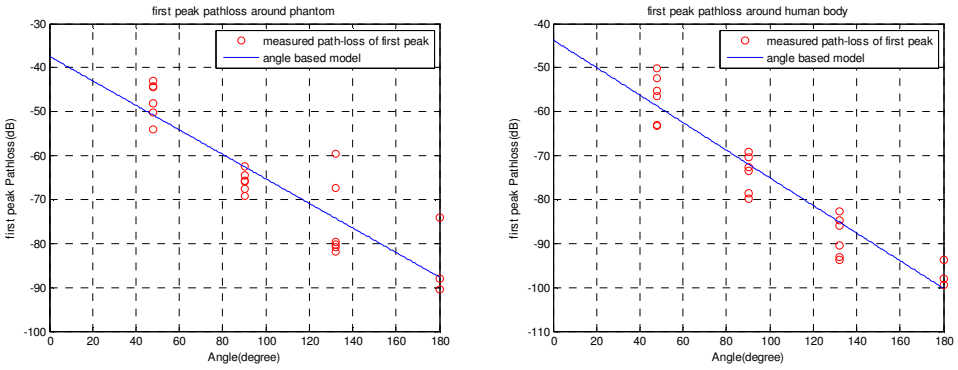

Figure 16: (a) Path-loss of the First Peak around the Phantom (b) Path-loss of the First Peak around Body

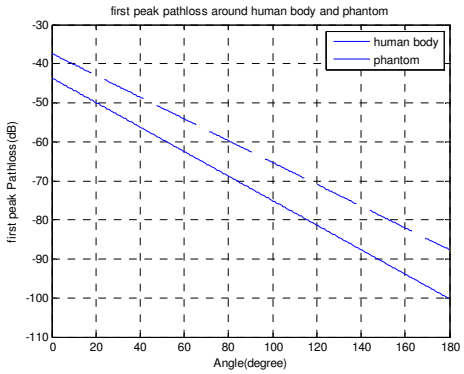

Figure 17: Compare the Angle based Channel Model around Body and Phantom

3.4.5Modeling the Total Path Loss

A channel model has been built in [18], which is suitable for UWB and based on the distance between the transmitter and the receiver. (14) is the distance based channel model. In our measurement the distance between the antenna and human body or the phantom is 10mm, so n is 6.0, d0 is 0.1m and P_{0dB} is 45.8dB. In this way, we can have the total path-loss of each point using this distance based channel model.

$$P_{dB} = P_{0dB} + 10n \log\left(\frac{d}{d_0}\right) \tag{14}$$

In the [38], the author builds channel models for wireless communication around human body along the degree of the angle between the transmitter antenna and receiver antenna in the radio frequency of 400MHz, 900MHz, and 2.4GHz. According our measurement result, we can build a channel model for RF localization around human body based on the degree of the angle between the transmitter and receiver in UWB as (15), which is an angle based channel model. The parameters used in this formula are shown in Table 7.

$$P_{dB}(\theta) = P_{dB}(\theta_0) - \gamma_1(\theta - \theta_0) \tag{15}$$

Table 7: Parameter of Angle Based Channel Model of the Total Path-loss

	Phantom	Human
$P_{dB}(\theta_0)$	36.25 dB	44.25 dB
γ_1	13dB/rad	16dB/rad
θ_0	0.3115 rad	0.3115 rad

Figure 18(a) and (b) show the measured total path-loss (circle point), the distance based channel model total path-loss (starlike point) and angle based channel model total path-loss (line) around a phantom and around human body. The vertical axis in Figure 18 is the angle between the transmitter and the receiver, and the horizontal axis is the total path-loss. In Figure 18, these two models for the total path-loss have been put together.

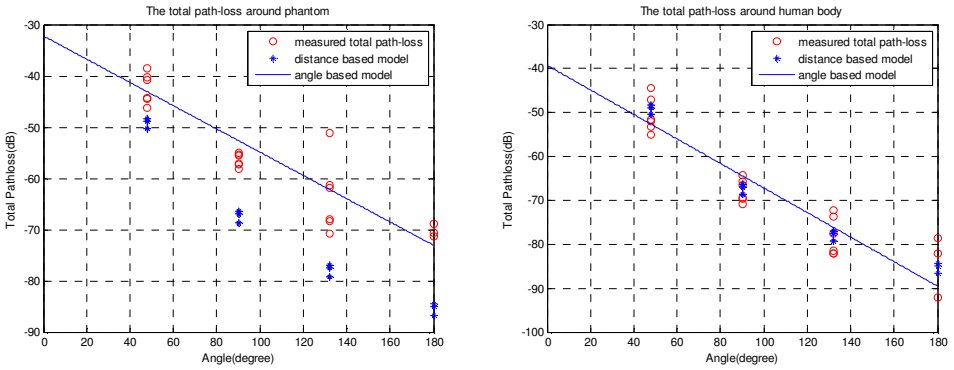

Figure 18: (a) Total path-loss around the phantom (b) Total path-loss around body

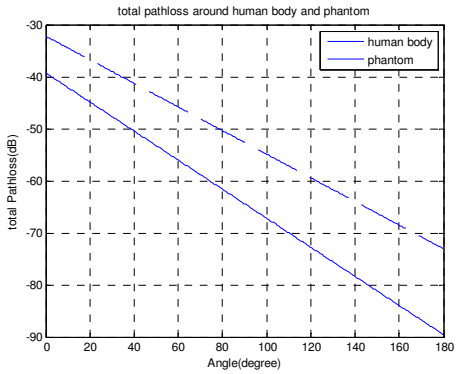

Figure 19: Compare the angle based channel model around body and phantom

Because our measurement results also have the distance information, we can calculate the path-loss gradient n using our measured path-loss of first peak based on the (9) which is built in [38], shown in Table 8. After fitting the measurement result we can get the path-loss gradient n equals to 5.8. And after analyzing the result of the measurement of total path-loss around a phantom, the path-loss gradient n equals to 4.47. The first path-loss gradient is larger than that of the total path-loss. So in this way the result we get about the path-loss gradient is reasonable.

Table 8: Path-loss Gradient n in Different Situation

	Path-loss gradient n	
	phantom	Human body
First-peak	5.8	7.27
Total path-loss	4.47	6

Chapter 4

UWB and NB Measurement in Homogenous Tissue

4.1 Introduction

In chapter 3, we have discussed the measurements and models around the human body for the mounted sensors. These models can help to provide the location information based on the receive RF signal for the body surface to body surface scenario. Additionally, researchers are also curious of the inside body environment, which is also very important to the implanted sensors for BAN. However, the inside human body is impossible, and we faced many challenges in the measurement with the phantom, including the antenna size and fixing the location of the antenna. Then we came to the idea of the homogenous tissue, which is a mimic of the environment inside the human body. This chapter describes of the measurement inside the homogenous tissue and the analysis of the result.

4.1.1Homogenous Tissue

Recent research related the homogenous tissue in [40] mentioned the narrowband measurement, but they only analyze the path-loss model. And in this thesis we will do the UWB measurement and compare the result with the narrowband one. This research is aiming to provide the location information. During the measurement in the CWINS lab, we made two

different kinds of homogenous tissue based on the related research [56-59]. The first physical model comprises mineral oil, a saline solution and an emulsifier. We are using the first kind of homogenous tissue to do the measurement in the tool box, which is shown in the last chapter, Figure 18. The second model of homogenous tissue is made of sugar, NaCl, HEC, bactericide and water. This homogenous tissue is non-oil so it is intended for more complicated measurements that will use the phantom. This part of measurement program will carried out in the future.

4.1.2Narrow Band

As we mentioned in the introduction, there are four frequency band used most for the BAN, and they are MICS (Medical Implant Communication Service), ISM (Industrial, Scientific and Medical), UWB (Ultra-Wide Band) and WMTS (Wireless Medical Telemetry Service). In this chapter we will analyze the implanted sensors. In order to compare the Distance Measurement Error of the UWB measurement result, we will also use the MICS band to do the measurement which is from 402-405 MHz range. And the frequency is allocated by the Federal Communication Commission (FCC). The MICS permits individuals and medical practitioners to utilize this mobile radio service which is ultra-low power [38]. The good characteristic of MICS includes the better propagation characteristic for implants and reasonable size of the antennas. Narrowband measurements are also always used in the indoor radio channel and also used to determine the Doppler spread of the indoor radio and human motions [22, 40]. In this chapter we proved that the phase of narrowband can be treated as a useful vector to provide location information.

4.2 Measurement Scenario

Firstly, I want to introduce the procedure that we build this measurement scenario. The environment inside the human body is kind of complicated for researchers to do the measurement. And we are trying to do the measurement inside the phantom which will be

filled homogenous tissue, but we have met some challenges. We cannot fix the antenna when we put it inside the phantom. Based on this situation, we decided to do the measurement inside the tool box filled with homogenous tissue instead.

This measurement setup is built for the measurement in homogenous tissue separately in UWB and Narrowband [41]. The measurements contain a flat box, a Vector Network Analyzer (VNA), UWB and narrowband antennas and we will give an introduction as follows.

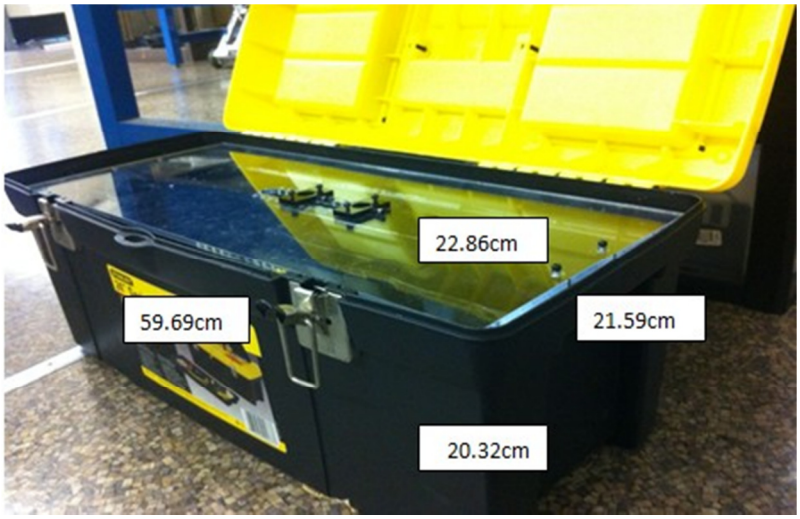

Figure 20: Flat Box for Measurement

All the measurements in this chapter were conducted in a flat box (59.69cm×21.59cm×20.32cm), Figure 20. During the measurement this flat box is filled with homogenous tissue which is a simply mimic environment of human body. The permittivity of the homogenous tissue is 81. In this way, the measurement inside this flat box can simply reflect the signal transmit situation inside human body. At the top of this flat box we placed a plastic plate which is used to hold the transmitter and the receiver. There are one hole and a slide in the plastic plate. The hole is used to fixed the transmit antenna, the slide is used for the receive antenna. The receiver can be moved 1cm by 1cm, in this way the distance between the transmitter and the receiver is from 2cm to 9cm. In this measurement scenario we can go ahead and do the measurement when the distance between the antennas is larger than 9cm, but when the distance is larger than 9cm, we cannot obtain the first peak of the signal which

means we cannot get the TOA of the first peak, so in this way we cannot obtain the location information.

All the measurements are using an E8363B Vector Network Analyzer (VNA), and the scenario including the VNA is shown in Figure 21. The parameters used in UWB are shown in Table 9, from which we can find the frequency swept is from 3GHz to 10GHz. We used a PC to store the measured transfer function (S21) which is wireless communicated with the VNA. The data we stored is in frequency domain. We used the MATLAB and to do the data analysis. When we analyze the UWB measurement results, we firstly use a Hamming Window to reduce the effects of side lobs and then covert the data from frequency domain to time domain using the Inverse-Chirp Z transform. We can easily obtain the first peak from time domain data by using a peak detection algorithm.

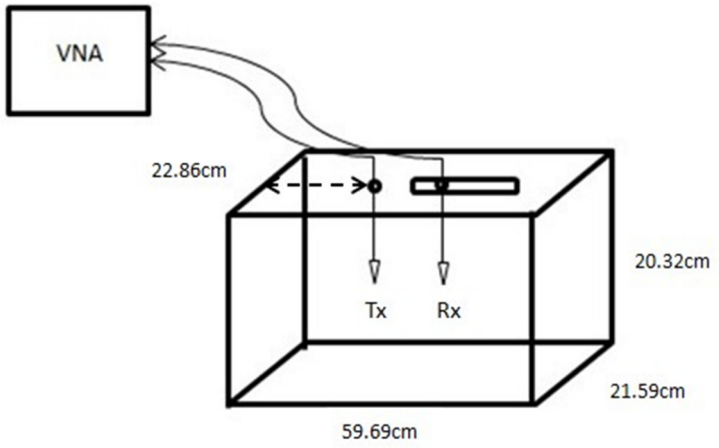

Figure 21: Measurement Scenario

Table 9: Measurement Parameters

VNA setup parameters	Value
Frequency band	3-10 GHz
Number of points	1601
Transmission power	0 dBm

The parameters for narrowband measurement are shown in Table 10. The central frequency is 402MHz. In the narrowband measurement, firstly we measure the S21 to calibrate the VNA then change the sweep type to CW (continue wave) Time. In this way, we can store a cti type file which include the time information and phase information. Because the data we store is in the CW, the data is already in time domain and no need to do the Fourier transformation. So in this way we can directly plot the phase of each point. And the measurement Parameters of UWB measurement are shown in Table 9, which is no difference with the measurement around the human body.

Table 10: Narrowband Measurement Parameters

VNA setup parameters	Value
Frequency band	402MHz
Number of points	1601
Sweep time	32 sec
Transmission power	0 dBm

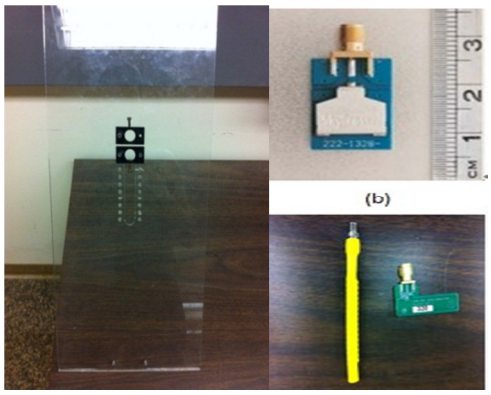

(a) (c)

Figure 22: (a) Plastic Plate; (b) UWB Antenna; (c) Narrowband Antenna

The plastic plate is shown in Figure 22 (a). By moving the receive antenna point by point, we can have the measurement information from 2cm to 9cm, 8 points totally. Additionally, to reduce the loss from the cables, Tin Foil is used to cover the cables as a better shielding. Compared with the measurement before using the Tin Foil, this better shielding is found working. The antennas we used in UWB measurement are SMT-3TO10M-A UWB patch antenna from SkyCross corporation[33]. The operating frequency range of this type of antenna is from 3.1GHz to 10.0 GHz, Figure 22(b). For narrowband measurement we use the ZL70102 antenna from Zarlink Semiconductor which operating frequency range is from 402 MHz to 405MHz, Figure 22(c) [42].

4.3 Measurement Result and Analysis

When people talking about the measurement inside the human body based on our imagination, there should be a lot of multipath inside the human body. But actually, after the comparison between the signal from the empty tool box and from the tool box filled with water, we found that the influence of the multipath inside the human body or the homogenous tissue may be not that serious.

4.3.1Multipath Situation Analysis

In order to figure out the multipath situation inside the human body, we have done the measurement in empty tool box and in the tool box filled with homogenous tissue. By compare these two measurement result, we will have a picture of the multipath situation inside the human body.

Figure 23 shows the multipath environment in an empty flat box. From this figure we can clearly find the five peaks with in 3ns. The straight lines show the expect TOA of these five different paths, which from direct path and reflection. The paths from reflection include the paths from the top and bottom of the flat box, from the two sides of the flat box. Compare the

expected TOA with the peaks we got from measurement, we can clearly found that these results have a good agreement. And Figure 24 is showing the measurement result when the antennas are in the same location with that in Figure 23. From Figure 24 we can find that there is only one peak which is the direct path and the power of the other multipath from the reflection are very close to the noise.

$$v(\omega) = \frac{c}{\sqrt{\varepsilon_{r(\omega)}}} \tag{16}$$

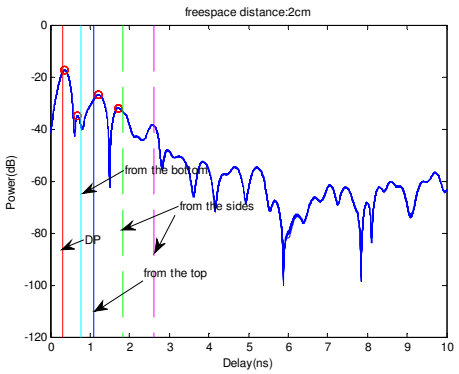

Figure 23: Multipath Situation in an Empty Flat Box

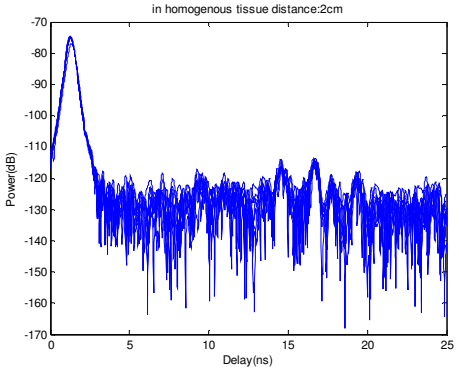

Figure 24: Multipath Situation inside Homogenous Tissue

Formula 16 shows the propagation velocity when signal transmits inside homogenous tissue [41]. And in our measurement the ε_r equals to 81, c is the speed of light. From the multipath situation in an empty flat box we can image the multipath situation in homogenous tissue. However, the paths from reflection in homogenous tissue have a huge path-loss during transmitting. The measurement results in homogenous tissue match the data analysis from the Figure 23 and Figure 24.

In order to show the multipath situation better, we also calculate the impulse respond in an empty flat box and flat box filled with homogenous tissue. Because the distance in these measurements is smaller than 1m, we have to use the original formula (17) to calculate the power in an empty flat box instead of formula (18) [18]. The impulse response in empty flat box is shown in Figure 25(a). From the data sheet of the antenna from Skycross, we can get the gains of the transmitter and receiver which are both 1.6.

$$\frac{P_r}{P_t} = G_t G_r \left(\frac{\lambda}{4\pi d}\right)^2 \tag{17}$$

$$L_p = L_0 + 20\log_{10}(d) \tag{18}$$

$$L_p = (10\log_{10} e^2)\alpha d + C \tag{19}$$

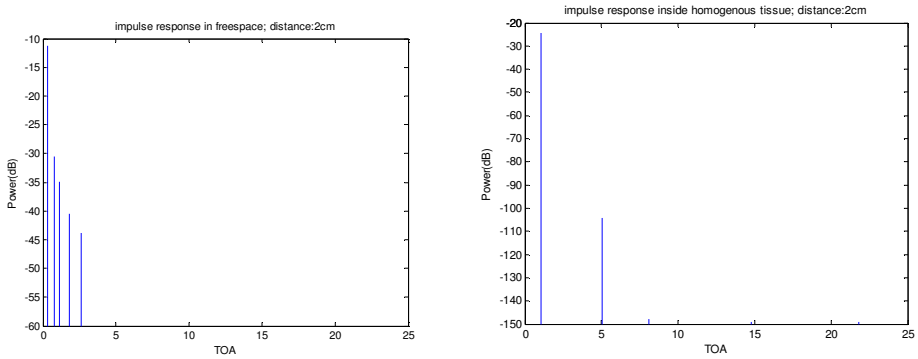

Figure 25: (a) Impulse Response in an Empty Flat Box (b) Impulse Response in Flat Box Filled with Homogenous Tissue

Table 11: Parameter for Path-loss Model

Parameters	α	C
Model 1	0.99	7.18
Model 2	0.66	15.79

From the formula (19) we can have the impulse response in flat box filled with homogenous tissue [40]. The parameters for formula (19) are shown in Table 11. When the distance is smaller than 2.78cm, model 1 is used to calculate the path-loss. When the distance is larger than 2.78cm, we use model 2.

Compare with these two impulse response shown in Figure 25 (a) and (b), we can find that the signals from different paths in homogenous tissue will influence each other less than that in empty flat box. Additionally, the path-loss of the reflections from the box is really huge and nearly same with the path-loss of the noise. Based on the analysis of the first peak we measured in S21 which is definitely from the direct path, we can have the conclusion that inside the homogenous tissue the multipath influence less than that in the empty flat box.

4.3.2UWB Measurement Result

In UWB measurement, we can use the TOA of the first peak, which is from the direct path, to obtain the location information. Firstly, to analyze the TOA of the first peak in UWB measurement, we have to eliminate the system bias which will have a really big influence of the accuracy of the localization. We do a measurement in homogenous tissue as a reference to calculate the system bias, and in this way we find the system bias in homogenous tissue Δt is 0.84 ns.

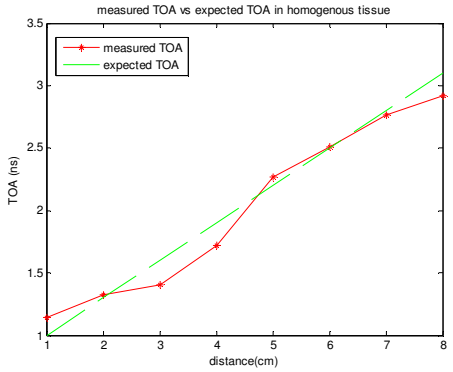

Figure 26: Measured and Expected TOA in Homogenous Tissue

Figure 26 shows the TOA of the first peak when the receiver moved 1cm by 1cm and in this way the distance between the transmitter and the receiver is changing from 2cm to 9cm. When the distance between the transmitter and receiver is less than 10 cm, the first path which is from the direct path is very obvious. Compare the expected TOA and the measured TOA from the Figure 24, we can find that these two have a good agreement and in this way the TOA of the first peak in UWB measurement can provide quite accurate location information.

4.3.3Narrow Band Measurement Result

In the narrowband measurement, we measured phase of the signal as the factor to get the localization information. Because when we choose the sweep type as CW (continue wave) Time, we cannot detect the first peak. The phase measurement result is shown in Figure 27. In Figure 27, the full line means expected phase of signal when the distance between the transmitter and receiver changing from 2cm to 9cm, and dots means the measured phase of each points.

Additionally, the phase of signal we measured through the VNA in CW Time model is the current phase of the signal instead of the phase defined in [18]. In this way we need to inverse the degree calculated by (20), (21) to the current degree. After the transformation we can compare the expected phase with the measured phase.

$$\emptyset = \frac{2\pi d}{\lambda} \tag{20}$$

$$\text{degree} = \emptyset \times \frac{180^\circ}{\pi} \tag{21}$$

The expected phase of signal calculated as the Formula 6, in which d means the distance between the transmitter and receiver, and λ means the wavelength in 402 MHz. However the result we obtained in this way is radian which is needed to be transfer in angle, (21).

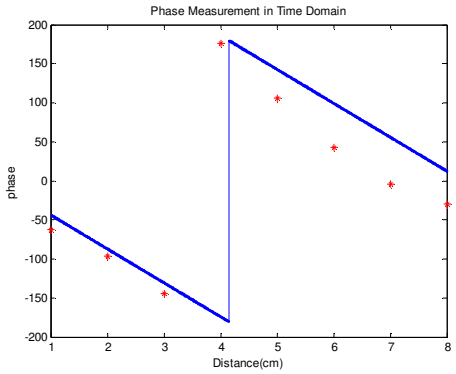

Figure 27: Measured and expected phase inside homogenous tissue

4.3.4Compare of the DME in UWB and Narrow Band

To figure out the localization accurancy of these two technologies TOA and POA in these two different bandwidth, UWB and Narrow band, we will analyze the DME (Distance Measurement Error) of the TOA and POA. The definition of DME is shown in Formula 17.

$$\varepsilon = \left|\hat{d} - d\right| \tag{22}$$

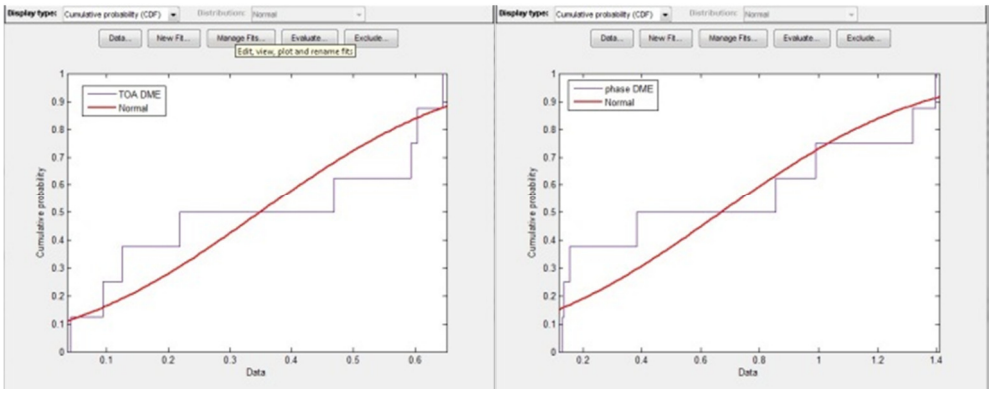

Figure 28: (a) CDF of DME of TOA in UWB Measurement (b) CDF of DME of phase in narrowband Measurement

The standard variance of DME of TOA in UWB measurement is 0.2548 cm. In this way, we can conclude that TOA technology for RF localization in UWB shows good performance. DME of TOA is defined as Formula (22). The CDF of DME of TOA in UWB measurement is shown in Figure 28(a) compared with Gaussian Distribution. In the phase measurement, the standard

variance of DME is 0.4837 cm, which is a little bit larger than that of DME of TOA. Based on the data we can tell that the phase of signal is a useful factor for RF localization in narrowband measurement. The CDF of DME of phase in narrowband measurement is shown in Figure 4.9(a), compared with Gaussian distribution.

From the phase measurement we can tell the trend of DME which is incresing with the increse of the distance between the transmit antenna and the receive antenna. In this way, we can tell that the location information provided by phase shows good performance, especially in short distance.

At the same time, we are continuing doing the measurement in the tool box which is filled with homogenous tissue in UWB and NB. Because in the homogenous tissue the multipath are much less than that in the free space, the DME for RF localization is smaller than that in free space from Figure 29 which is a really good news for the applications in BAN. Based on the measurement result, we found that the DME of the measurement in UWB inside the homogenous tissue is the smallest, and then the second smallest is DME of the phase of the signal in Narrowband inside the homogenous tissue. Based on which we can conclude that inside the homogenous tissue where the multipath influence less, we will obtain the less error in the measurement.

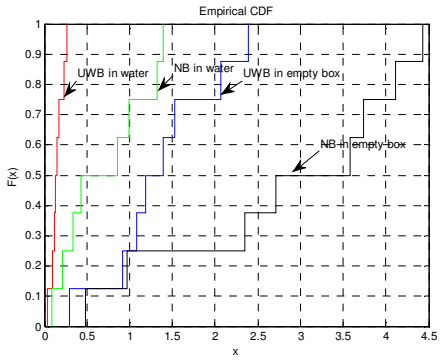

Figure 29: CDF of DME in Four Different Environments

4.4 Effects of Antenna Bandwidth

During the measurement inside the homogenous tissue, we observe the change of the antenna bandwidth inside the liquid. The width of the pulse inside the homogenous tissue is narrower than that in the free space. Based on this observation, we want to analyze the effects of antenna bandwidth. Firstly, we have done the measurements inside the homogenous tissue and analyzed the S11 result. The measurement results of S11 in free space and homogenous tissue are shown in Figure 30 (a) and (b). From Figure 30, we can find the useful bandwidth in the free space is from 4GHz to 8.8GHz, but in the homogenous tissue the useful bandwidth changes to 8GHz to 10GHz. This result is under the assumption that we take the -10dB as the threshold. The useful bandwidth is dramatically changed.

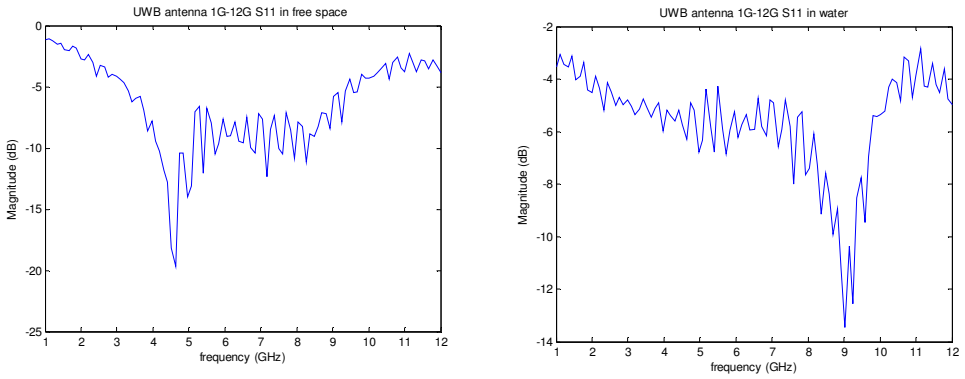

Figure 30: (a) S11 Measurement of Antenna Bandwidth in free space (b) S11 Measurement of Antenna Bandwidth in Homogenous Tissue

To solid this assumption, we design the measurement of S21 to analyze the antenna bandwidth. The measurement results of S21 in free space and homogenous tissue are shown in Figure 31(a) (b) and Figure 32 (a) and (b). These measurements help us to analyze the effects of the environment and distance. We measure the S21 when the distance between the transmitter and receiver is 3cm and 10cm. From these measurement results we can find that the big difference in bandwidth when the UWB antenna in different environments. Additionally, by comparing the Figure 31(b) and Figure 32(b) we can find the distance between

the transmit antenna and the receive antenna may have an influence for the antenna bandwidth.

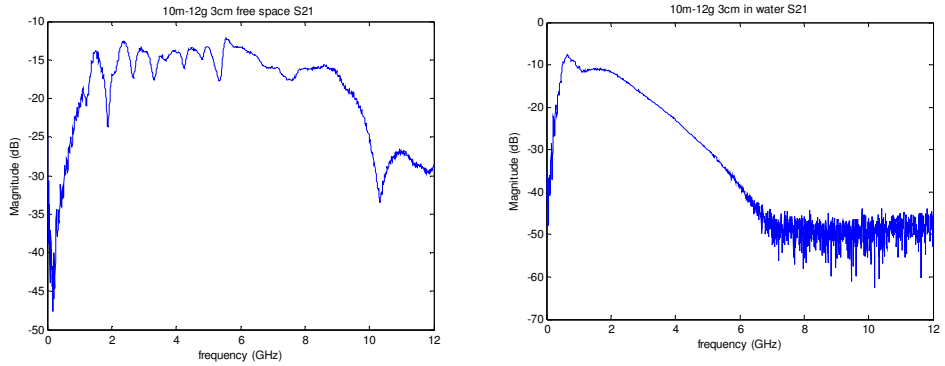

Figure 31: (a) S21 Measurement of Antenna Bandwidth in free space(3cm) (b) S21 Measurement of Antenna Bandwidth in Homogenous Tissue(3cm)

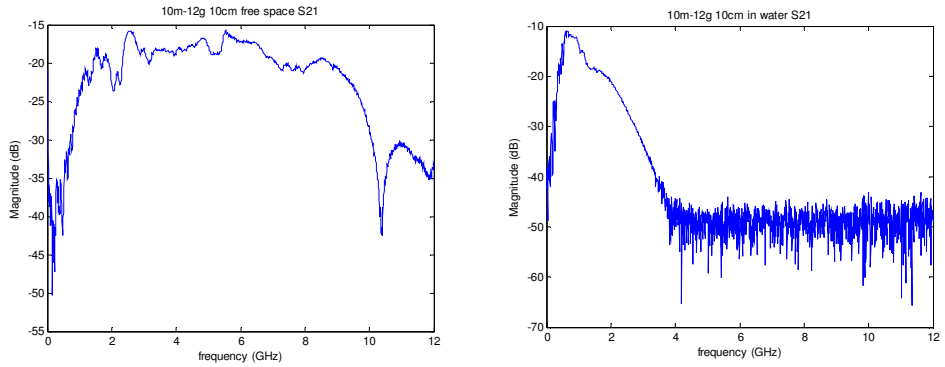

Figure 32: (a) S21 Measurement of Antenna Bandwidth in free space(10cm) (b) S21 Measurement of Antenna Bandwidth in Homogenous Tissue(10cm)

Chapter 5

Conclusion and Future Work

In this thesis, we have focused on research in UWB characteristics of RF localization for BANs operating around the human body and inside the human body. Based on our measurement results, we found that when the mounted sensors are fixed around the human body, the signals are propagating as creeping waves. Additionally, we constructed a channel model for TOA, total path-loss and power of the first peak based on angle.

Following our investigation of propagation around the human body, we addressed the case of propagation inside the human body. Given that is impractical to perform measurements inside the human body, we chose to make measurements using a model of homogenous tissue, to mimic the environment inside the human body. First, the multipath situation was analyzed. Comparing the measurement result for an empty tool box and the tool box filled with homogenous tissue, we found that the observed multipath influence was less inside the homogenous tissue. Then we made measurements inside the homogenous tissue at UWB and narrowband frequencies. We measured the TOA of the UWB signal and phase of narrowband signal. Based on the measurement result we found that when we eliminate the influence of the multipath the DME of localization is reduced.

With the help of the simulation software, SEMCAD X, we will compare the measurement result with the simulation result and found the limitation of the bandwidth and distance in the future. And additionally, we will do the non-homogenous simulation to figure out for the implant to implant scenario for BAN. I and Yishuang will also continue the project cooperated with the UCLA medical school analyzing several metrics, the Doppler spread and RMS spread of the firefighter's motions.

References

[1] "First Report and Order 02-48", Federal Communications Washington, DC, 2002.

[2] Nader Bargshady, Nayef A. Alsindi, Kaveh Pahlavan, Yunxing Ye and Ferit Ozan Akgul, "Bounds on Performance of Hybrid WiFi-UWB Cooperativc RF Localization for Robotic Applications", 2010 IEEE 21st International Symposium on PIMRC Workshops, pp.277-282.

[3] Andrew Fort, Claude Desset, Philippe De Doncker, Piet Wambacq and Leo Van Biesen, "An Ultra-Wideband Body Area Propagation Channel Model—From Statistics to Implementation" in IEEE TRANSACTIONS ON MICROWAVE THEORY AND TECHNIQUES, VOL. 54, NO. 4, APRIL 2006.

[4] Julien Ryckaert, Claude Desset, Andrew Fort, Mustafa Badaroglu, Vincent De Heyn, Piet Wambacq, Geert Van der Plas, Stéphane Donnay, Bart Van Poucke, and Bert Gyselinckx, "Ultra-Wide-Band Transmitter for Low-Power Wireless Body Area Networks:Design and Evaluation", in IEEE TRANSACTIONS ON CIRCUITS AND SYSTEMS—I: REGULAR PAPERS, VOL. 52, NO. 12, DECEMBER 2005.

[5] Andreas F. Molisch, Dajana Cassioli, Chia-Chin Chong, Shahriar Emami, Andrew Fort, Balakrishnan Kannan, Johan Karedal, Juergen Kunisch, Hans Gregory Schantz, Kazimierz Siwiak, and Moe Z. Win, "A Comprehensive Standardized Model for Ultrawideband Propagation Channels". In IEEE TRANSACTIONS ON ANTENNAS AND PROPAGATION, VOL. 54, NO. 11, NOVEMBER 2006.

[6] Kenichi Takizawa, Hiroaki Hagiwara and Kiyoshi Hamagach. "Path_loss estimation of wireless channels in capsule endoscopy from Xray CT images" 33rd Annual international conference of the IEEE EMBC, Boston, Massachusetts, August 30-September 3, 2011

[7] Pranay Swar, Master Thesis, "On the Performance Evaluation of In-Body RF Localization Techniques", 2012.

[8] Shen Li, Master Thesis, "A Hardware Platform for Wireless Access and Localization Performance Evaluation of Devices inside the Human Body", 2012.

[9] Umair Khan, Master Thesis, "Computational Techniques for Comparative Performance Evaluation of RF Localization inside the Human Body", 2011

[10] Laurens Roelens, Wount Joseph, Elisabeth Reusens, Gunter Vermeeren and Luc Martens, “Characterization of Scattering Parameters Near a Flat Phantom for Wireless Body Area Networks” in IEEE Transactions on Electromagnetic Compatibility, Vol. 50, No.1, February 2008.

[11] L. Roelens, S. Van den Bulcke, W. Joseph, G. Vermeeren and L. Martens, “ Path loss model for wireless narrowband communication above flat phantom”, in Electronics Letters, 5th January 2006 Vol. 42 No.1.

[12] Developing Wireless Body Area Network Standard, IEEE 802.15 WPAN™ Task Group 6 (TG6). http://www.ieee802.org/15/pub/TG6.html

[13] Sana Ullah, Henry Higgins, Bart Braem, Benoit Latre, Chris Blondia, Ingrid Moerman, Shahnaz Saleem, Ziaur Rahman, Kyung Sup Kwak, “*A Comprehensive Survey of Wireless Body Area Networks*”, in Journal of Medical Systems, June 2012, Volume 36, Issue 3, pp 1065-1094.

[14] Yunxing Ye, Umair Khan, Nayef Alsindi, Ruijun Fu and Kaveh Pahlavan, “*On the accuracy of RF positioning in multi-Capsule endoscope*” in IEEE International Symposium Personal, Indoor and Mobile Radio Communication (PIMRC), 2011.

[15] The global positioning system: a shared national asset: *recommendations for technical improvements and enhancements.* National Academies Press. p.16. ISBN 0-309-05283-1., Chapter 1, p. 16, 1995

[16] "*Factsheets: GPS Advanced Control Segment (OCX)*". Losangeles.af.mil. October 25, 2011. Retrieved November 6, 2011.

[17] Kaveh Pahlavan and Allen H. Levesque, “*Wireless Information Networks*”, second edition, Chapter 13, pp. 610. ISBN-13 978-0-471-72542-8, 2005.

[18] Kaveh Pahlavan & Prashant Krishnamurthy, “*Principles of Wireless Networks: A Unified Approach*”, 2002.

[19] FCC Rules and Regulations, “*MICS Band Plan*”, Part 95, Jan. 2003.

[20] ZL70102 Application Development Kit, http://www.zarlink.com.

[21] "*industrial, scientific and medical (ISM) applications (of radio frequency energy): Operation of equipment or appliances designed to generate and use locally radio*

frequency energy for industrial, scientific, medical, domestic or similar purposes, excluding applications in the field of telecommunications." International Telecommunication Union. 19 October, 2009. 1.15.

[22] Ruijun Fu, Yunxing Ye, Ning Yang and Kaveh Pahlavan, "*Doppler Spread Analysis of Human Motions For Body Area Network Applications*", in IEEE International Symposium Personal, Indoor and Mobile Radio Communication (PIMRC), 2011.

[23] A. Tronquo, H. Rogier, C. Hertleer and L. Van Langenhove, "Robust planar textile antenna for wireless body LANs operating in 2.45GHz ISM band", in ELECTRONICS LETTERS, 2nd February 2006, Vol. 42, No.3.

[24] "*FCC statement on coexistence of WMTS and other frequency bands*", http://wireless.fcc.gov

[25] "*UWB Technical Overview*", Track IT System White Paper.

[26] M. Steinbauer, A.F. Molisch, and E. Bonek, "*The Double Directional Mobile Radio Channel*," IEEE Antennas and Propagation Magazine, vol. 43, no. 4, pp. 51–63, Apr. 2001.

[27] Jun-ichi Takada, Takahiro Aoyagi, Kenichi Takizawa, Norihiko Katayama, Takehiko Kobayashi, Kamya Yekeh Yazdandoost, Huan-bang Li, and Ryuji Kohno, "*Static Propagation and Channel Models in Body Area*", EUROPEAN COOPERATION IN THE FIELD OF SCIENTIFIC AND TECHNICAL RESEARCH COST 2100 TD(08)639 Lille, France, 2008/Oct/6-8.

[28] Takahiro Aoyagi, Jun-ichi Takada, Kenichi Takizawa, Hirokazu Sawada, Norihiko Katayama, Kamya Yekeh Yazdandoost, Takehiko Kobayashi, Huan-Bang Li, and Ryuji Kohno, "*Channel Models for WBANs – NICT*", 29 September, 2008.

[29] Kamya Yekeh Yazdandoost and Kamran Sayrafian-Pour, "*Channel Model for Body Area Network (BAN)*", 27 April, 2009.

[30] Aravind Kailas, Mary Ann Ingram. "*Wireless Aspects of Telehealth*", Wireless Pers Commun (2009) 51:673-686.

[31] A. Fort, J. Ryckaert, C. Desset, P. Dpncker and P. Wambacq, "*Ultra-Wideband Channel Model for Communication Around the Human Body*", in IEEE Journal on Selected Areas in Communication, Vol.24, No.4, April 2006, pp.927-933.

[32] Umair I. Khan, Kaveh Pahlavan, Sergey Makarov, "*Comparision of TOA and RSS Based Techniques for RF Localization inside Human Tissue*" in 33rd Annual International Conference of the IEEE EMBS, 2011, pp. 5602-5607.

[33] SkyCross,online, Available: http://www.skycross.com

[34] Phantom Laboratory, online, Available: http://www.phantomlab.com/

[35] Kaveh Pahlavan, Yunxing Ye, Umair Khan and Ruijun Fu, "RF localization Inside Human Body: Enabling micro-robotic navigation for medical applications", in Localization and GNSS(ICL-GNSS), 2011 International Conference, June 2011, pp. 133-139.

[36] Sinan Gezici, Zhi Tian, Georgios B. Giannakis, Hisashi Kobayashi, Andreas F. Molisch, H. Vincent Poor, and Zafer Sahinoglu, "Localization via Ultra-Wideband Radios" in IEEE SIGNAL PROCESSING MAGAZINE, July 2005, pp. 70-84.

[37] Jin Chen, Yunxing Ye, Kaveh Pahlavan, "*UWB Characteristics of Creeping Wave for RF Localization around the Human Body*" in in IEEE International Symposium Personal, Indoor and Mobile Radio Communication (PIMRC), 2012.

[38] Kamran Sayrafian-Poue, Wen-Bin Yang, John Hagedorn, Judith Terrill, "*A Statistical Path Loss Model for Medical Implant Communication Channels*", in Personal, Indoor and Mobile Radio Communication (PIMRC), 2009 IEEE 20th International Symposium.

[39] Steven J.Howard, Kaveh Pahlavan, "*Fading Results From Narrowband Measurement of the Indoor Radio Channel*", in Personal, Indoor and Mobile Radio Communication (PIMRC), IEEE International Symposium, 1991.

[40] D. Kurup, W.Joseph, G. Vermeeren and L. Martens, " *Path loss model for in-body communication in homogeneous human muscle tissue*", in Electronics Letters, 2009

[41] Makoto Kawasaki, Ryuji Kohno, "*A TOA based Positioning Technique of Medical Implanted Devices*".

[42] Zarlink, online, Available: http://www.zarlink.com

[43] Schmid & Partner Engineering (SPEAG) , "SEMCAD-X Manual"

[44] U. Khan, K. Pahlavan, Umair Khan, "Computational Techniques for Comparative Performance Evaluation of RF Localization inside the Human Body" , 2011.

[45] P. Swar, K. Pahlavan and U. Khan, "Accuracy of localization system inside human body using a fast FDTD simulation technique" , Medical Information and Communication Technology (ISMICT), La Jolla, CA, USA, March, 2012

[46] J. He, Y. Geng and K. Pahlavan, "*Modeling indoor TOA Ranging Error for Body Mounted Sensors*", 2012 IEEE 23nd International Symposium on Personal Indoor and Mobile Radio Communications (PIMRC), Sydney, Australia Sep. 2012

[47] S. Li, Y. Geng and K. Pahlavan, "*Analysis of Three-Dimensional Maximum Likelihood Algorithm for Capsule Endoscopy Localization*", 5th IEEE International Conference on Biomedical Engineering and Informatics, Chongqing, China Oct. 2012.

[48] S.L. Cotton and W.G. Scanlon, "*Characterization and Modeling of On-body Spatial Diversity within Indoor Environments at 868 MHz*", IEEE Transactions on Antennas and Propagation, vol.8, no.1, pp. 14-18, Feb. 2009.

[49] S.L. Cotton, G.A. Conway and W.G. Scanlon, "*A Time-Domain Approach to the Analysis and Modeling of On-body propagation Characteristics Using Synchronized Measurements at 2.45 GHz*", IEEE Transactions on Antennas and Propagation, vol.57, no.4, pp. 943-949, Apr. 2009.

[50] A.F. Molisch, J.R. Foerster and M. pendergrass, "*Channel models for ultra wideband personal area networks*", IEEE wireless communications magazine, pp.14-21, Vol.10, Issue.6, 2003.

[51] A. Fort, C. Desset, J. Ryckaert, P.D. Doncker, L.V. Biesen and P.Wambacq, "*Characterization of the ultra-wideband body area propagation channel*", 2005 IEEE International Conference on Ultra-Wideband, Zurich, Switzerland Sep. 2005.

[52] D. Smith, L. Hanlen, D. Miniutti, J. Zhang, D.Rodda and B. Gilbert, "*Characterization of the Dynamic Narrowband On-body to Off-body Area Channel*", Applied Sciences on Biomedical and Communication Technologies, pp. 1-5, Oct. 2008.

[53] D. Smith, D. Miniutti, L. Hanlen, D.Rodda and B. Gilbert, "*Dynamic Narrowband Body Area Communications: Link-Margin Based Performance Analysis and Second-order Temporal Statistics*", 2010 IEEE Wireless Communications and Networking Conference, Sydney, Australia Apr. 2010 .

[54] R. Fu, Y. Ye, N. Yang and K. Pahlavan, "*Doppler Spread Analysis of Human Motions for Body Area Network Application*", 2011 IEEE 22nd International Symposium on Personal Indoor and Mobile Radio communications (PIMRC), Toronto, Canada Sep. 2011.

[55] J. He, Y. Geng and K. Pahlavan, "Modeling indoor TOA Ranging Error for Body Mounted Sensors", 2012 IEEE 23nd International Symposium on Personal Indoor and Mobile Radio Communications (PIMRC), Sydney, Australia Sep. 2012.

[56] Michael Y. Kanda, Maurice Ballen, Sheldon Salins, Chung-Kwang Chou and Quirino Balzano, "*Formulation and Characterization of Tissue Equivalent Liquids Used for RF Densitometry and Dosimetry Measurements*", in IEEE TRANSACTIONS ON MICROWAVE THEORY AND TECHNIQUES, VOL. 52, NO. 8, AUGUST 2004.

[57] A. Peyman and C. Gabriel, "*Development and characterisation of tissue equivalent materials for frequency range 30–300MHz*", ELECTRONICS LETTERS 1st March 2007 Vol. 43 No. 5.

[58] "*Full Body Custom Liqui-Phil™ M a n u a l*", from Phantom lab.

[59] GLENN S. SMITH, WAYMOND R. SCOTT. JR, "*The Use of Emulsions to Represent Dielectric Materials in Electromagnetic Scale Models*", lEEE TRANSACTIONS ON ANTENNAS AND PROPAGATION. VOL. 38, NO. 3. MARCH 1990.

[60] Zhuoran Liu, Jin Chen, Umair Khan and Kaveh Pahlavan, "*Effects of Bandwidth and Distance on TOA in non-Homogenous Tissue*", 2013 IEEE 23nd International Symposium on Personal Indoor and Mobile Radio Communications (PIMRC), London, England Sep. 2013.

[61] Yishuang Geng, Jin Chen and Kaveh Pahlavan, "*Analysis of Narrow Band Propargation Characteristic for the First Responder*", 2013 IEEE 23nd International Symposium on Personal Indoor and Mobile Radio Communications (PIMRC), London, England Sep. 2013.

Appendix A

A.1 Measurement results around phantom

When the receiver antenna is in point 1:

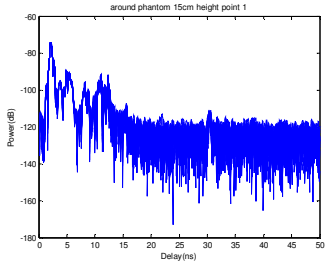

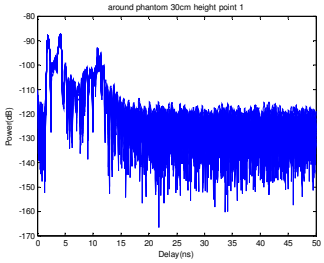

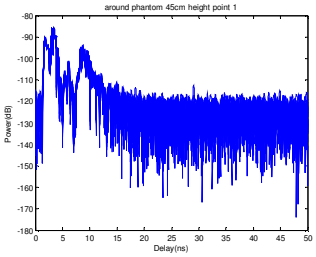

When the receiver antenna is in point 2:

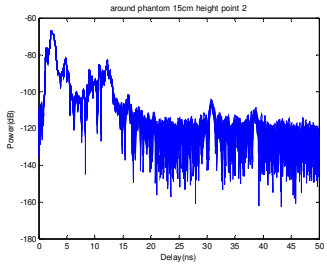

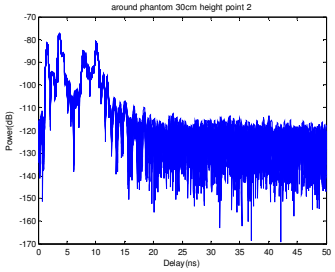

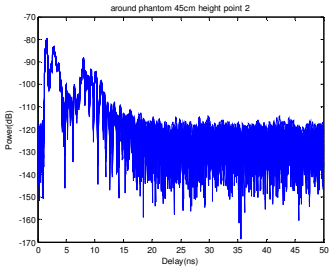

When the receiver antenna is in point 3:

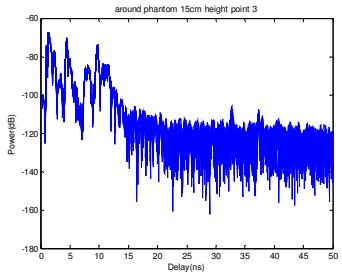

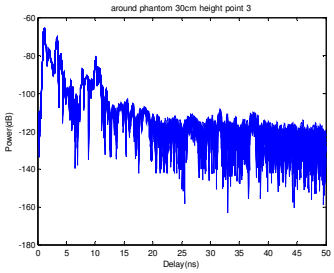

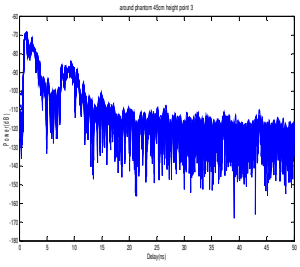

When the receiver antenna is in point 4:

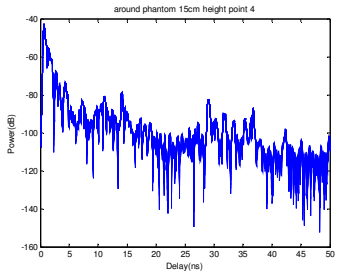

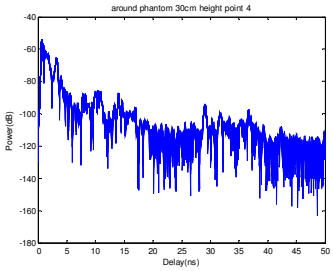

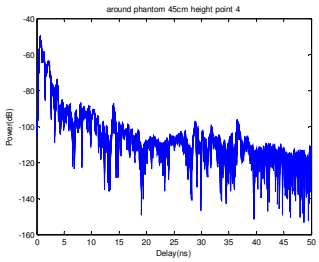

When the receiver antenna is in point 5:

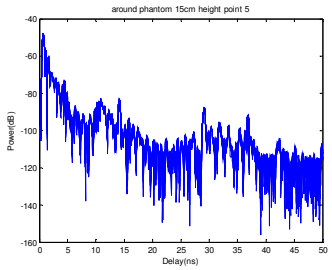

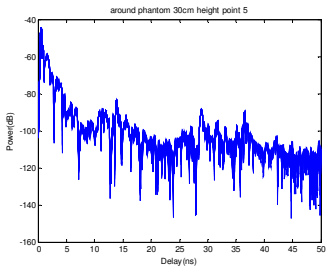

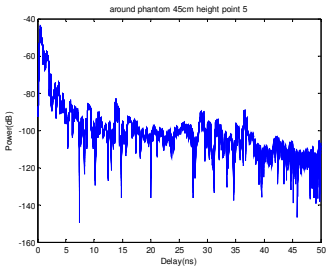

When the receiver antenna is in point 6:

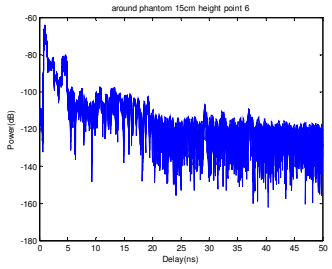

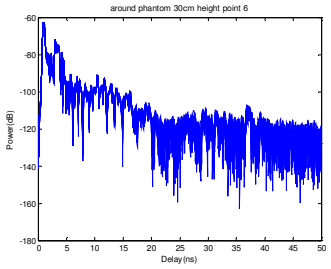

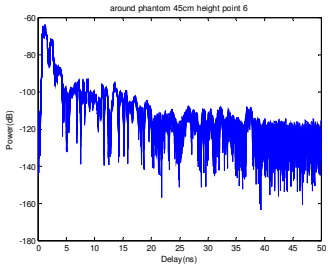

When the receiver antenna is in point 7:

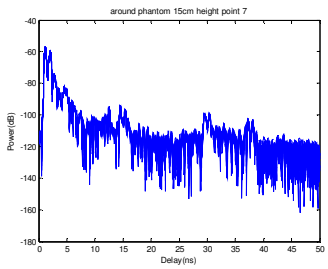

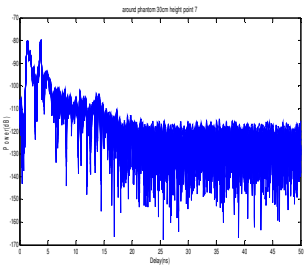

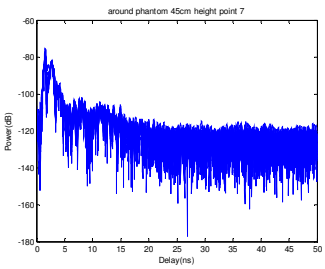

A.2 Measurement results around human body

When the receiver antenna is in point 1:

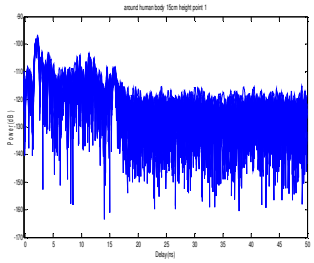
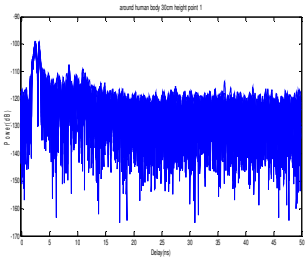
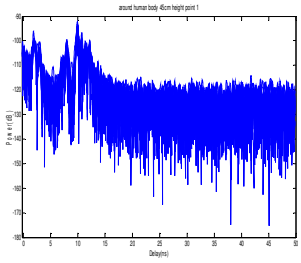

When the receiver antenna is in point 2:

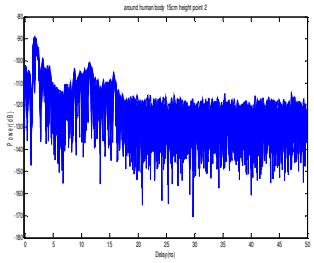
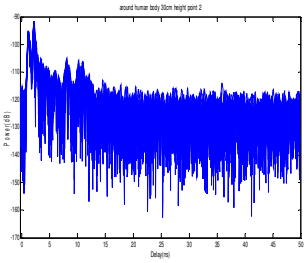
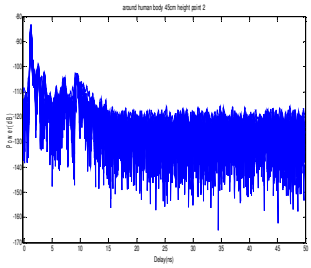

When the receiver antenna is in point 3:

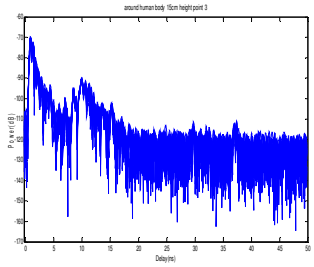
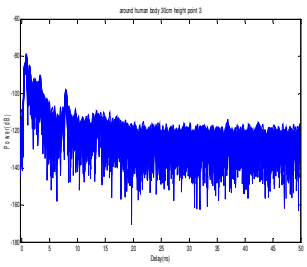
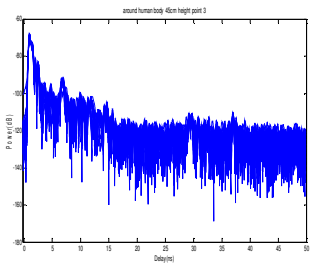

When the receiver antenna is in point 4:

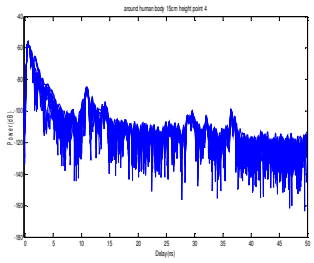
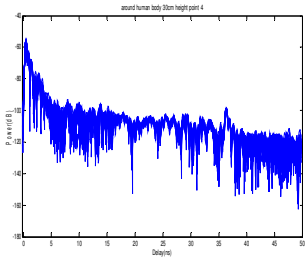
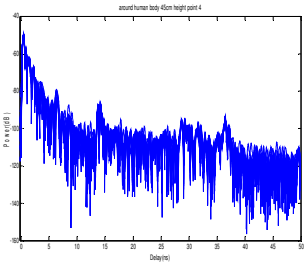

When the receiver antenna is in point 5:

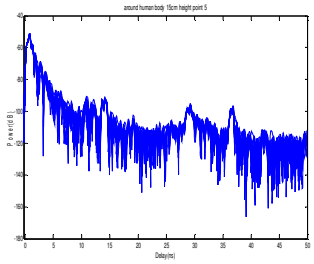
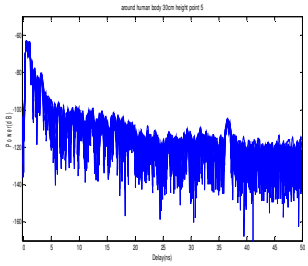
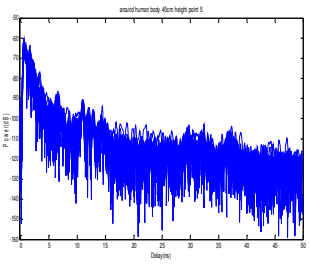

When the receiver antenna is in point 6:

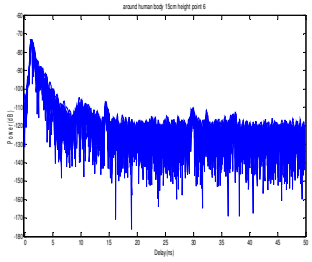
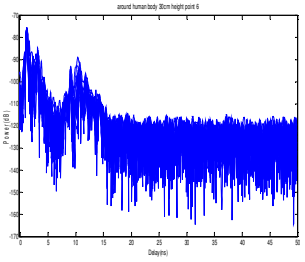
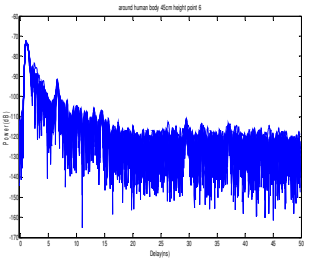

When the receiver antenna is in point 7:

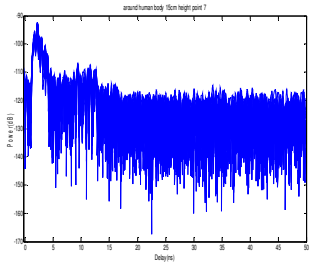
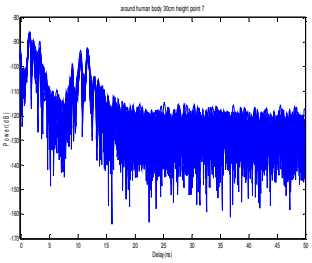
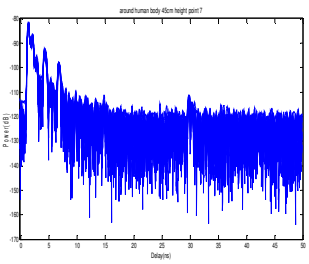

Appendix B

Simulation vs Measurement

B.1 Introduction

In this chapter, we have done the measurements in different bandwidth, from 50MHz to 7GHz, and different distances between transmitter and receiver inside the homogenous tissue, from 2cm to 6cm. Additionally, we have simulated the homogenous tissue environment using SEMCAD X, a software that is used to solve electromagnetic and wireless issues based on Finite Difference Time Domain (FDTD) algorithm. We then compared the simulation results with the measurement results after we get them. Based on these results, we analyzed the limitations and effects of bandwidth and distance inside the homogenous tissue.)

With the high increase of the human age all over the world, people pay more and more attention on the human health. BAN (Body Area Network) describes the application of wearable computing devices, which focus on the channel propagation around, on and inside the human body [12]. In many application of the BAN, the data from the sensor is useless without the location information. Wireless Capsule Endoscopy (WCE), for example, needs the image processing to provide the location information, with which the doctor can find where the bleeding or infection is [14].

There are several technologies can provide the location information. The most normal ones is based on the TOA (Time of Arrival) and the RSS (Receive Signal Strength). Some other technologies includes TDOA (Time Difference of Arrival), RTT (Round Trip Time) and AOA (Angel of Arrival) [17].

UWB technology has attracted much attention after the Federal Communication Commission (FCC) unlicensed 3.1 to 10.6 GHz for UWB communication applications [1], even though it doesn't meet the expected results. For the BAN applications, the characteristics of UWB are helpful because of its low battery cost, high data rate and high central frequency. Recent research has found that UWB shows good performance in RF localization around human body using Creeping wave [37].

SEMCAD X is a kind of simulation software aimed to solve the electromagnetic and wireless issues in terms of antenna design and Electromagnetic Compatibility (EMC) based on Finite Different Time Domain (FDTD) algorithm, provided by Schmid & Partner Engineering (SPEAG). This software provides a wide range of anatomical inhomogeneous human body models to help better solve the electromagnetic and wireless waveform transmission problems in or around human body. What is more, this software has a relatively higher simulation running speed than other normal electromagnetic simulation software with the help of aXware Accelerate card and aXware ClusterInABox introduced in mid-2009 [44].

FDTD method is first proposed by Yee in 1966. This Algorithm solves Maxwell's curl equations in time domain. FDTD has been proven to be an effective simulation method that it calculates the field parameters accurately. Simulations based on FDTD method has been used in many application fields such as indoor localization and microwave applications. As we all know that it is difficult to do measurements inside human body because its non-homogeneous environment and human body motion, we can hardly know the waveform transmission situation there. SEMCAD X simulations based on FDTD helps us to conquer this challenge. We can simulate the environment inside human body and put antennas inside the model to get the results we want. In this project we proved that SEMCAD X simulations are accurate and reliable in Body Area Networks after comparing with the measurement results.

B.2 Simulation Scenario

In order to better compare the simulation results with measurement results. We built up a plastic box model that the size is identical to the flat box for the measurement. Its length, width and height are 59.69cm, 21.59cm and 20,32cm respectively. The plastic box is filled with homogeneous tissue whose permittivity is 81. The solid material of the box is polyethylene and its permittivity is 2.25. In the simulation, transmitter and receiver are dipole antennas. The impedances of dipole antennas are both 50Ω. The amplitude of the input voltage signal is set to be 1V.

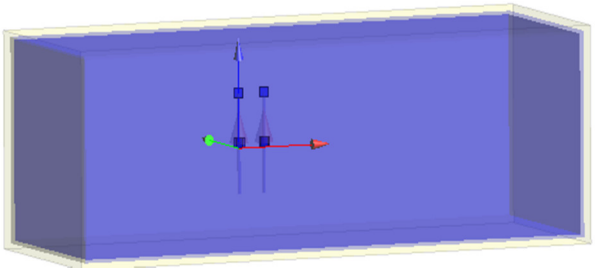

Figure 33: Flat Box Model for Simulation

Being identical to the measurement settings, the central frequency of the system is 6.5MHz and the bandwidth ranges from 50MHz to 7GHz. Based on the voltage and impedances provided, the transmit power of this system is 10dBm. For the purpose of making better comparison between measurement and simulation results, we added a 10dB calibration on the measurement results.

To simulate the input from Vector Network Analyzer, we use the hanning window as the input signal. The spectral characteristic of the hanning window is showed as following the Formula (23), where β, the roll-off factor can be between 0 and 1. Its corresponding time-domain Nyquist pulse is given by Formula (23)

$$\{f(t)\} = \begin{cases} T, & 0 \le |f| \le \frac{1-\beta}{2T} \\ \frac{T}{2}\left[1 - \sin\frac{\pi T}{\beta}(|f| - \frac{1}{2T})\right], & \frac{1-\beta}{2T} \le |f| \le \frac{1+\beta}{2T} \end{cases} \quad (23)$$

$$f(t) = \frac{\sin\pi t/T}{\pi t/T} \times \frac{\cos\beta\pi t/T}{1-4\beta^2t^2/T^2} \quad (24)$$

T is the interval between two zero-valued points [44]. In our simulations, we pick 1 to be the value of β.

What we have to pay attention to is that the central frequency of the measurement signal is 6.5GHz while the frequency domain of hanning window is even symmetry, which means the central freuqency of hanning window is zero. We have to shift the central frequency of the hanning window from 0 to 6.5GHz by multiplying a cosine at the end of Eq. (25), the cosine function is given by

$$\cos(2\pi \times 6.5 \times 10^9 t) \quad (25)$$

In SEMCAD X, we can easily get the S-parameters of 2-port networks. By doing the Inverse Chirp-Z transform of the S21 parameter we can get the impulse response of the system.

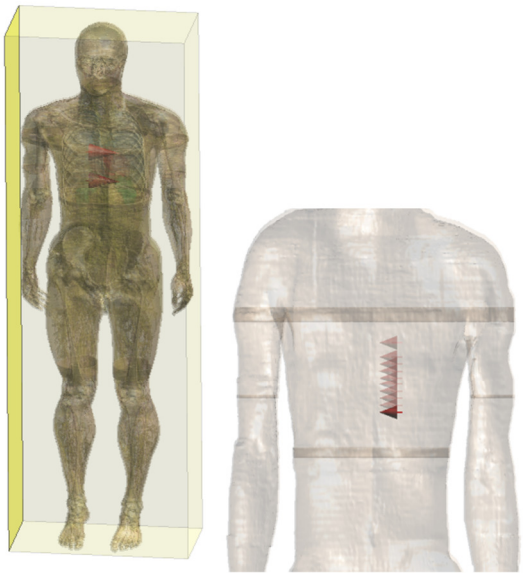

Figure 34: the Human Body Model (Left); Layout of Transmitted and Received Sensors (Right)

On the other hand, we simulated in-body waveform transmission. We imported a model of a 34-year old man and put two sensors inside human body at the location of human torso. In these simulations, we put the transmit sensor at one place and move the receiver sensor one centimeter by one centimeter away from the transmitter. The distance between two sensors ranges from 2cm to 10cm. The human body model is showed as Figure 34.

B.3 Verification of SEMCAD X

From the previous studies [45], we already know that simulation system based on FDTD method is an LTI system. To make full use of SEMCAD X, which is based on FDTD algorithm, we must verify that the FDTD simulation system in SEMCAD X is reliable. We simulated the homogeneous tissue measurement at different bandwidth and distances and compared them with measurement result to check how well they fitted each other.

As we compared the simulation results of homogenous tissue with measurement results at different bandwidth. We can see from Figure 5 that the simulation and measurement results are very close under the bandwidth of 400MHz. Thus we conclude that simulation fits measurement well in homogeneous tissue under the bandwidth of 400MHz with a grid size of 0.16mm.

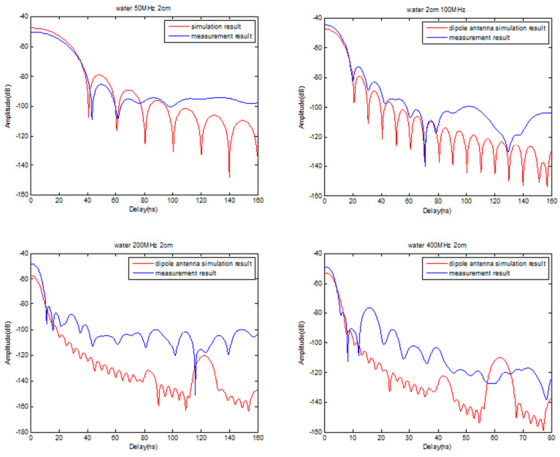

Figure 35: Analysis of Bandwidth Limitation

After we have confirmed that the SEMCAD X simulation is reliable, we want to know the effect of distance on Time-of-Arrival (TOA) in homogeneous tissue. We have done the measurement at 50MHz of different distances from 2cm to 6cm in water.

During the measurement, we collected ten groups of data at each distance. As Figure 36 shows, there are ten measurement result points and one simulation result points at each distance. We can know from Figure 36 that the difference on amplitude of received signal and TOA between measurement and simulation is very small when the distance is smaller than 6cm. We noticed that at the distance of 6cm, the TOA of measurement result is 36.7ns and the average of received signal amplitude is -80dB which are way inaccurate. We can get the result that the distance limitation in water is 6cm at the bandwidth of 50MHz. We can also get the equation of the linear relationship between amplitude and logarithmic of distance from the left one of Figure 36:

$$\mathrm{L} = -136.9 \times \log(\mathrm{d}) - 3.9 \tag{26}$$

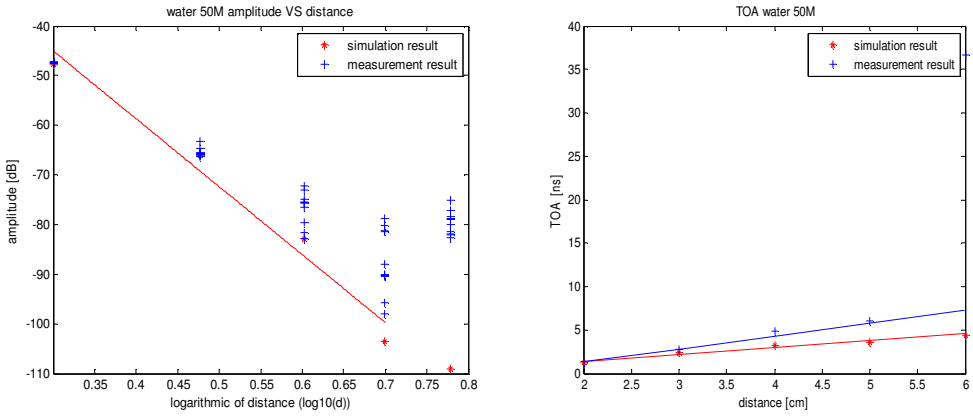

Figure 36: Amplitude Versus Distance (left) and TOA Versus distance at 50MHz in water (right)

We can calculate Distance Measurement Error (DME) of both measurement and simulations from the results of Figure 37. Equation 27 shown as follows gives the method to calculate DME:

$$\varepsilon = \left| \mathrm{t} \times \frac{\mathrm{c}}{\sqrt{\varepsilon_\mathrm{r}}} - \mathrm{d} \right| \tag{27}$$

Where ε is DME, ε_r is the relative permittivity and d is the actual distance, c is the speed of light and $\frac{c}{\sqrt{\varepsilon_r}}$ is the velocity in water. We use detected TOA multiply by the velocity in water and minus the actual distance then we get the DME. Figure 37 shows the DME of measurement and simulation at different distance respectively.

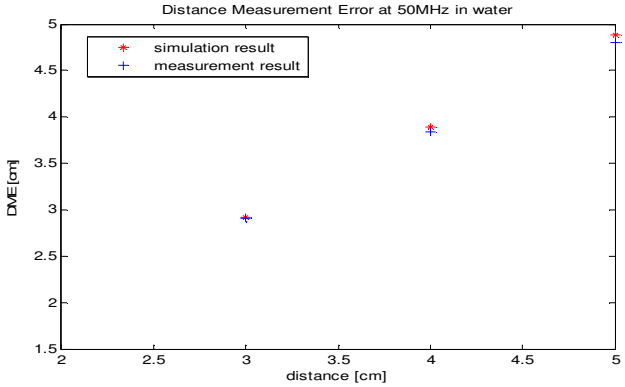

Figure 37: DME at 50MHz in water

Appendix C

Doppler Spread Analysis of Firefighter Motions for BAN

C.1 Introduction

The rapid advancement in wireless technology, implantable medical devices and pervasive computing gave birth to a booming era of body area network (BAN) and BAN is finding an increasing number of applications in different fields such as clinical treatment, health care, social security and even entertainment [46] [47]. One of the most distinguished applications for BAN is the real-time on-body health monitoring networks. Such monitoring network consists of a set of low power, small size, wearable sensors measuring physiological signal of the objective and a central unit that collects recorded data from sensors through the wireless connection. Smart phones and PDAs are often selected as the central unit for their natural wireless functionality, computational capability and access to wide area network. Among numerous available wireless access technologies, bluetooth is one of the most promising candidate for the connection between physiological sensor and central unit due to the fact that adaptive frequency hopping spread spectrum (AFHSS) used in bluetooth limits the interference with other networks, low power consumption of Bluetooth guarantees the battery life, the ISM band and the well-developed bluetooth modules make the system implementation affordable. Since for any communication system, the ultimate limits on system performance is the channel it operates in, the wireless channel on the surface of human body attracts increasingly attention in both academic and industry. IEEE 802.15.6 Task Group 6 is officially working on the standardization for on-body wireless channel and it focus on multiple issues from path-loss model to cyber

security [12]. In the open literature, researches related to propagation characteristics of the on body radio frequency (RF) signals focused on multiple frequency band (such as MISC, ISM, WMTS and UWB) [48] [49] and various environments (such as free space, typical office room and hospital room) [50] [51]. Most of the past papers concentrated on the statistical characterization of channels for given scenario by attaching a probability density function (PDF) or second-order statistics including fading duration and level crossing rate [52] [53]. There is also previous research on Doppler spread and RMS Doppler bandwidth by analyzing time domain channel profile of simple human motions [54]. Previously mentioned statistical models are easy-to-use and computationally efficient in general and they perform very well for the health monitoring system designed for patients in the hospital. However, when the monitoring systems are assigned to first responders working in harsh environment, throughput and reliability of the system drops drastically. Statistical models suffer the lack of accuracy due to the fact that most of them are derived from extensive measurement results which are not specific to the intended deployment condition and environment. First responder in this project denotes to the person who has completed a course and received certification in providing pre-hospital care for medical emergencies such as police officers, firefighters and etc. Take the firefighters as an example, when they work in a burning house, both their equipment and fire-proof clothing has a strong influence on the on-body wireless channel and such channel is extremely critical.

In this chapter, to address the issue, measurements have been conducted inside an anechoic chamber with the objective wearing standard fire-proof clothing and equipment such as mask and hat. The transmitter is fixed to the left trouser pocket while receiver located at different location on the surface of human body. Single tone has been transmitted and time domain channel profile has been recorded to calculate the path-loss. The path-loss is observed to be higher than the common scenario without firefighter's equipment, indicating a requirement of higher transmit power to guarantee the same performance. Doppler spread is calculated with frequently appeared motion of firefighter. The Doppler spread is defined as the width of received spectrum when the single tone waveform has been transmitted, which includes the information of fading rate of the channel [54]. With the Doppler spread in different

human motion, we have the potential ability to identify the status of firefighters, thus providing better protection to the first responder working in harsh environment.

This work is supported by Wireless Health Monitoring and Location Tracking, Rapid Product Development Center (UCLA subcontract No. 1562-S-PD386), which is sponsored by US Department of Interior/DHS. This work has been also performed under the American Recovery and Reinvestment Act Measurement, Science and Engineering Grants program (NIST Grant No. 60NANB10D001), which is sponsored by the National Institute of Standards and Technology (NIST). This part of project is cooperated with Yishuang Geng in CWINS.

C.2Measurement Scenario and Result

The empirical measurement for wireless channel from body surface to body surface has been performed in an anechoic chamber with the size of 2.32m×2.41m×2.29m which shield the reflections and avoid outside signals. The measurement system employed in this project consists of a vector network analyzer (VNA, Agilent E8363), a pair of low loss cable, and a pair of small size ISM quarter wavelength antenna. A medium size male has been selected as the objective of the measurement. The transmitter antenna has been attached to the trouser pocket at the height of 0:89m and it is connected to the TX port of VNA while the receiver antenna has been connected to the RX port of VNA and it has been located at different on-body locations throughout the measurement. The VNA continuously sent out single tone waveform at the frequency of 2.45 GHz. The S-parameter S21, which is also known as the channel transfer function or channel forward gain has been measured by the VNA in time domain to get the signal strength of the received single tone. Since the antenna-body interaction is an integral part of the overall propagation characteristic, the influence of antenna has been included as part of the channel. For every 20sec, the VNA samples the received signal strength (RSS) of the single tone at a rate of 80 samples per second, therefore the upper bound of measurable Doppler Shift is 40Hz with a frequency resolution of 0:012Hz. In the measurement the center frequency is 2.45

GHz, the sample point number is 1601, sweep time equals to 20s, and the transmit power is 0 dBm.

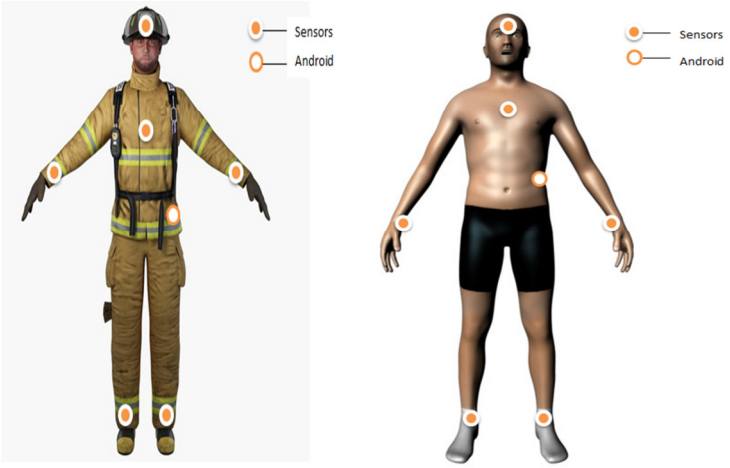

Figure 38: Sketch of the fire-proof clothing and equipment employed in the measurement including a coat and a mask

From the perspective of scenario-based approach, a measurement case set can be denoted by:

Case = {Clothing, Motion, TX, RX};

Subset Clothing indicates if the objective wears the fire-proof staff or not and is given by:

Clothing = {Equipped, NonEquipped};

The NonEquipped element represents the case that the objective wears common clothes and the Clothing subset is also shown in Fig36. In the Motion subset, we consider seven frequently appeared motions for firefighters and the subset is given by:

Motion = {Standing, Walking, Running, Lying, Climbing, Crawling, OnTheStair}

Only respiratory and palpitation occur when the human body is in Standing and Lying scenario and objective is expected to periodically move his arms and feet in proper scale in Climbing and Crawling scenario. The firefighters usually move very fast when going up or down stairs so that in Running and onTheStair scenario, the objective move his arms and feet quickly

and the scale is larger than Climbing and Crawling. Subset TX represents the location of transmitter antenna that is fixed to the left trouser pocket and it denotes to:

TX = {LeftPocket};

Subset RX indicates the multiple possible location of receiver antenna and is given by

RX = {Chest, Forehead, RightWrist, RightAnkle};

Based on the above definitions, a specific case of our measurement can be:

Case = {Equipped, Running, LeftPocket, Chest};

1) Path-loss: As for the path-loss of the on-body wireless channel, we recorded the time domain channel profile with the Motion subset set to Standing and rest of the subsets traversal all their elements. The empirical results can be therefore partitioned into two classes by whether the objective wears the fire-proof equipment or not. As a result, effects of the fire-proof equipment can be identified.

2) Doppler Spread: As for the Doppler Spread of the on-body channel in different motions, since the Doppler Spread only depends on the relative velocity of transmitter and receiver, we set the Clothing subset to Equipped and let rest of the subsets traversal all their elements. Consequently, the Doppler Spread can be classified by the motion of objective.

Table 12: Coefficients for the Near Boday UWB Model

	Chest	Right Wrist	Right Ankle	Front head
NonEquipped	56.5659dB	58.3729dB	62.1638dB	63.8422dB
Equipped	58.2771dB	61.3061dB	65.7988dB	67.3843dB

To obtain the average path-loss of the single tone, 10 snapshots have been recorded from each measurement case in the case set given by:

Case1 = {Clothing1, Motion1, TX, RX1}

Clothing1 = {Equipped, NonEquipped}

Motion1 = {Standing}

TX = {LeftPocket}

Rx1 = {Chest, Forehead, RightWrist, RightAnkle}

where each snapshots contains 1601 samples of the RSS and the average path-loss is given by:

$$P_l(Case) = -20\log_{10}\left(\frac{1}{N_s}\frac{1}{N_f}\sum_{i=1}^{N_s}\sum_{n=1}^{N_f}H(f_c;t)\right) \quad (28)$$

where $\mathrm{P_l(Case)}$ is the average path-loss for specific case, $\mathrm{N_s}$ is the number of snapshots which is 10 in this project, $\mathrm{N_f}$ is the number of frequency sample points in each snapshot which is 1601 and H($\mathrm{f_c}$; t) is the time domain S21 reading at each sample point from the VNA. By our design, the narrow band path-loss is independent from the human motion. The observation based on empirical measurement results is that the narrow band path-loss of the on-body channel for first responder varies from 55.4347dB to 69.1074dB according to the multiple locations of the receiver antenna. Comparison between the Equipped and NonEquipped case shows that the effects of fire-proof equipment results in a 2.9554dB greater average path-loss and 0.2324dB larger fluctuation. Empirical measurement results are also listed in table 12. Since the RF signal travels on the surface of human body in the pattern of creeping wave, linear regression fitting can be applied to the measurement results and the path-loss can be modeled in terms of distance between transmitter and receiver as:

$$P_L(d) = L_0 + 10\alpha\ \log_{10}(d) + S \quad (29)$$

where the $P_L(d)$ denotes to the path-loss of the narrow band signal, L_0 = 68.43dB represents the path-loss at reference distance of 0mm, α= 2.463 is the path-loss exponent indicating the

fading rate of the channel and S ~ (0,1.93dB) is the variation term of path-loss. Since the model in equation (29) is based on regression fitting, it can be used as reference model with tolerable error from inaccuracy in calculation and irregular edges of body surface. However, from a scientific point of view, they should only be used for specific receiver antenna locations for which the underlying measurements are valid.

As is known to all, whenever a relative motion between transmitter and receiver occurs, there will be an sharp change of frequency in radio systems. If the wave source and the receiver are moving toward each other, higher frequency signal will be detected at the receiver side due to the fact that the receiver receives greater number of wavefront per unit time and upward frequency shift is applied to the original signal. In the opposite, when the wave source and the receiver are moving away from each other, lower frequency signal will be detected at the receiver since the number of wavefront per unit time becomes less and a downward frequency shift will be added.

The maximum Doppler Shift f_m is given by the relative velocity of transmitter and receiver v_c and the signal wave length $= \frac{c}{f_c}$ as

$$f_m = \pm \frac{v_c}{\lambda} \tag{30}$$

where c = 3 × 108m/s represents the speed of light in free space and f_c represents the center frequency of transmitted signal. f_m remains positive whenever upward frequency shift occurs, otherwise it will be negative. Since the Doppler Spread represents the temporal variation of the on-body channel and it is caused by the relative movement of transmitter and receiver, we assume that the channel we operates in can be represented by wide sense stationary (WSS) process at a minimum. The Doppler Spread D(λ) can be obtained by applying a fast Fourier transform (FFT) to the recorded time domain channel response H(fc; t) as:

$$\mathrm{D}(\lambda) = \int_{-\infty}^{\infty} \mathrm{H}(\mathrm{f_c}; \mathrm{t}) \mathrm{e}^{-\mathrm{j}2\pi\mathrm{t}} \, \mathrm{dt} \tag{31}$$

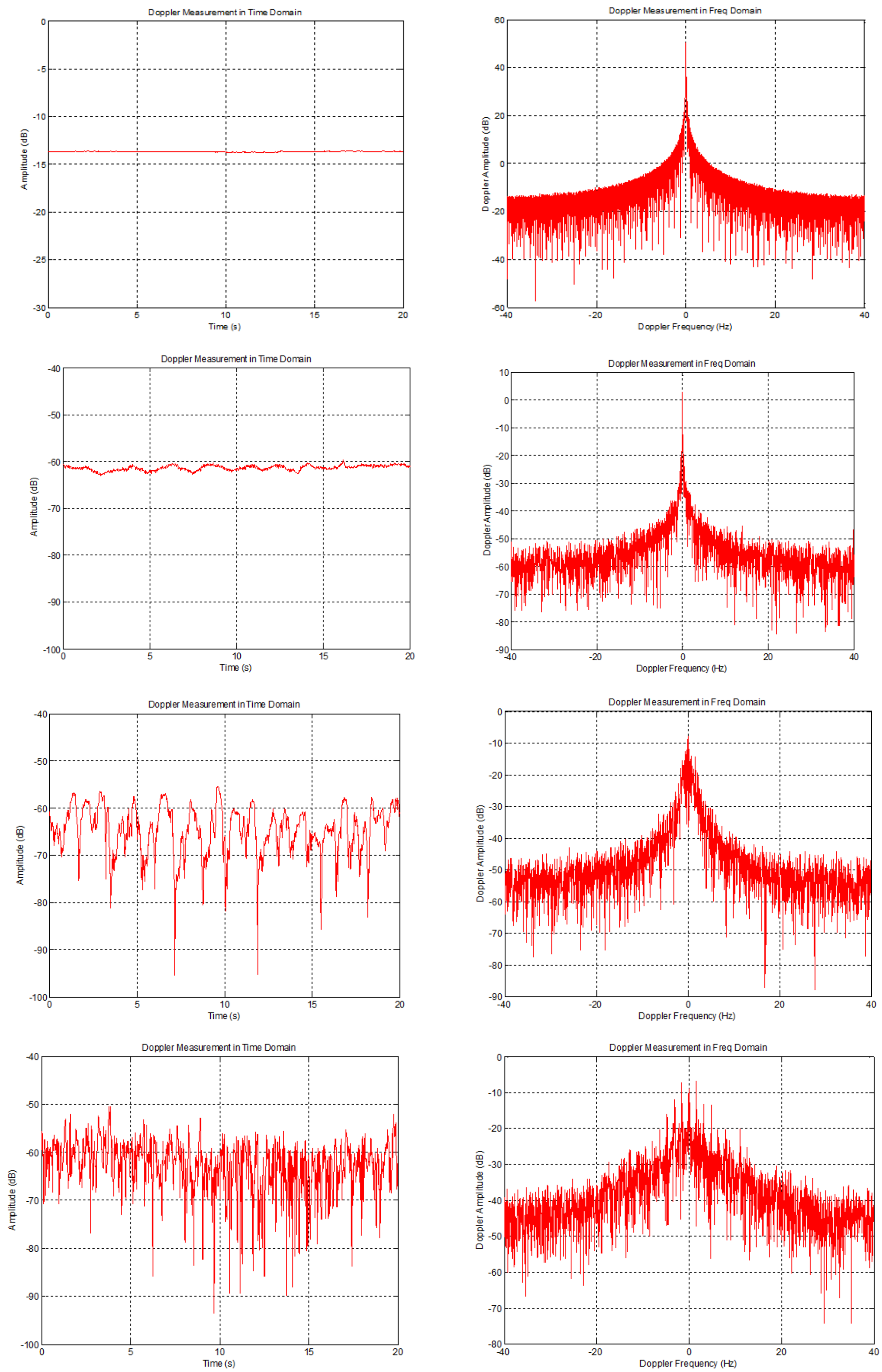

Doppler Measurement in Time Domain
Amplitude (dB)
Time (s)
Doppler Measurement in Freq Domain
Doppler Amplitude (dB)
Doppler Frequency (Hz)
Doppler Measurement in Time Domain
Amplitude (dB)
Time (s)
Doppler Measurement in Freq Domain
Doppler Amplitude (dB)
Doppler Frequency (Hz)
Doppler Measurement in Time Domain
Amplitude (dB)
Time (s)
Doppler Measurement in Freq Domain
Doppler Amplitude (dB)
Doppler Frequency (Hz)
Doppler Measurement in Time Domain
Amplitude (dB)
Time (s)
Doppler Measurement in Freq Domain
Doppler Amplitude (dB)
Doppler Frequency (Hz)

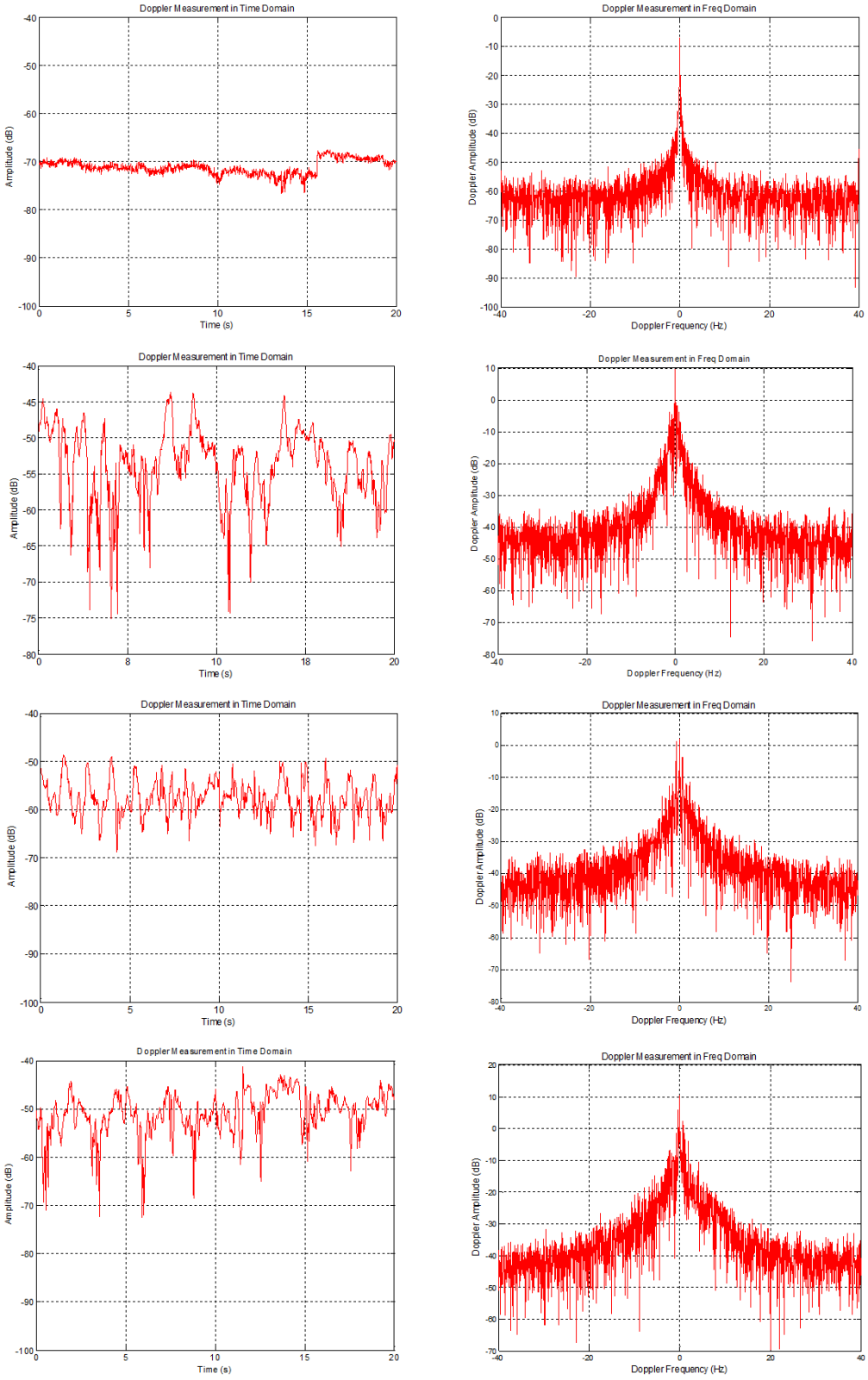

Figure 39: Time Domain Frequency Profile and Frequency Domain Doppler Spread

A threshold of -25dBm has been also applied to the frequency domain Doppler Spread D(λ) to get the final reading of Doppler Spread. A set of measurement results of Doppler Spread has been depicted in Fig. 39 including both time domain channel response H(fc; t) and frequency domain channel response D(λ). It shows the specific measurement results from the case set given by:

Case2 = {Clothing2, Motion2, TX, RX2}

Clothing2 = {Equipped}

Motion2 = {Standing, Walking, Running, Lying, Climbing, Crawling, OnTheStair}

TX = {LeftPocket}

Rx2 = {RightWrist}

Table 13 lists the overall Doppler Spread based on our scenario set. It comes to the conclusion that the Doppler Spread varies from 0.1539Hz to 18.0884Hz in respect of the motion of the human body as well as location of receiver antenna. By horizontal comparison among human motion, for Standing and Lying cases, the minimum Doppler Spread can be observed as low as 0.1539Hz while for Running and OnTheStair cases, the maximum Doppler Spread goes up to 18.0884Hz. By vertical comparison among different receiver antenna location for same human motion, we observe that when receiver antenna is located at the Chest, the Doppler Spread remains below 14.1345Hz for all human motion, indicating that the Doppler Spread is closely related to the movement intensity of the place we attach the receiver antenna.

Table 13: Doppler Spread

	Standing	Walking	Running	Lying	Climbing	Crawling	OnTheStair
Chest	0.6762	6.1679	13.8729	0.2412	8.4454	11.3828	14.1345
ForeHead	0.9024	7.8492	16.3059	0.1539	8.3526	12.3591	15.0358
Right Wrist	0.8785	9.0138	16.2475	0.3462	9.7325	12.3526	15.6891
Right Ankle	0.9116	11.3414	17.3895	0.1917	11.1893	13.9251	18.0884

In this chapter, empirical measurement has been conducted to obtain the narrow band characteristic of the specific case of first responder. The basic equipment and clothing for fire-fighter have been taken into consideration. With the transmitter antenna fixed to the left

trouser pocket, effects of different locations of receiver antenna on channel path-loss have been discussed. Apart from that, Doppler Spread has been also analyzed which is induced by seven continuous human motions. Since nowadays, the classification algorithms are in the limelight and many mature algorithms such as support vector machine (SVM) and neural network are proposed, the future work of this research will be focusing on the classification of the body motion by using available RF metrics such as path-loss and Doppler Spread.